Fe(III) oxide microparticles modulate extracellular electron transfer in anodic biofilms dominated by bacteria of the Pelobacter genus

Timothé Philippon, Fatima-Zahra Ait-Itto, Alicia Monfort, Frédéric Barrière, James A Behan

Fe(III) oxide microparticles modulate extracellular electron transfer in anodic biofilms dominated by bacteria of the Pelobacter genus.

Timothé Philippon, Fatima-Zahra Ait-Itto, Alicia Monfort, Frédéric Barrière*, James A. Behan*

Université de Rennes, CNRS, Institut des Sciences Chimiques de Rennes, UMR 6226, Rennes, France

**Corresponding authors:* james.behan@univ-rennes1.fr

frederic.barriere@univ-rennes1.fr

Abstract

Exo-electrogenic organisms have been extensively studied for their ability to transfer electrons with solid surfaces using a large variety of metabolic pathways. Most of the studies on these organisms consist in the replacement of solid electron acceptors such as Fe(III) oxides found in nature by electrodes with the objective of generating harvestable current in devices such as microbial fuel cells. In this study we show how the presence of solid ferric oxide (Fe_2O_3) particles in the inoculum during bio-anode development influences extracellular electron transfer to the electrode. Amplification and sequencing of the 16S rRNA (V4-V5 region) show bacteria and archaea communities with a large predominance of the *Pelobacter* genus, which is known to be phylogenetically close to the *Geobacter* genus, regardless of the presence or absence of ferric oxide in the inoculum. Data indicate that the bacteria at the bio-anode surface can preferentially utilize solid ferric oxide as terminal electron acceptors instead of the anode, though extracellular electron transfer to the anode can be restored by removing the particles. Mixed inoculum commonly used to develop bioanodes may produce similar bacterial communities with divergent electrochemical responses due to the presence of alternate electron acceptors, with direct implications for microbial fuel cell performance.

Keywords: Electroactive biofilms, Ferric oxides, 16S rRNA gene sequencing, *Pelobacter*, Microbial fuel cells, Bioanodes

1. Introduction

The development of exo-electrogenic biofilms is the subject of intense research due to their potential applications within microbial fuel cells (MFCs) and other bioelectrochemical systems [1–6]. There has been considerable focus on the development of bioanodes, i.e. the development of biofilms of exo-electrogenic organisms capable of extracellular electron transfer (EET) to solid electron acceptors such as metal oxides using electrons obtained through oxidation of organic matter via their respiratory metabolism [3, 7–12]. This interest has been motivated in large part by the prospect of harnessing microbial fuel cells for the depollution of wastewaters [13–15] and as green power sources, especially for low-power devices such as environmental probes and sensors [16].

One of the most important goals in bioanode research is the optimization of catalytic current generation at the anode, which requires the consideration of many factors including the choice of electrode material and its surface chemistry [2, 6, 17–20], the inoculum [5, 7, 21, 22], and the particular incubation conditions employed [23, 24]. The inoculum is among the most important factors for two reasons: firstly, without specific bio-augmentation, exo-electrogenic biofilms can only be obtained via selective pressure from the diverse bacterial communities originally present in the milieu (commonly soil, garden compost or waste water). Hence, bio-anode development from mixed inoculum requires the selection of specific bacteria with adaptations (such as redox shuttles, outer membrane proteins or conductive pili [8, 25]) which can facilitate EET to solid electron acceptors. Secondly, the physico-chemical properties of the inoculum determine the nutrient and mineral profile, including the presence of ferric oxides (e.g. magnetite, hematite) and manganese IV oxides (e.g. MnO_2) [26, 27] which are among the most important naturally-occuring solid terminal electron acceptors available to potential exo-electrogens.

Typically, the capacity to reduce solid oxides by such bacteria also facilitates electron transfer to an external electrode and the production of current, though this is not necessarily always the case [28]. Moreover even for bacteria known to be capable of EET, such as those of the *Geobacter* genus, the composition of the growth media as well as specific growth conditions employed during biofilm formation can dramatically affect the properties of the resulting biofilm [23, 24, 29]. The inoculum composition itself has also been shown to directly affect the measured electrochemical response of exo-electrogenic biofilms [7], however to our knowledge, despite the fact that exo-electrogens are often isolated from natural environments rich in solid electron acceptors, the specific effect of enriching the natural inoculum with alternative solid electron acceptors on anodic exo-electrogenic biofilm development has not been investigated. In this

work we present a study of bio-anode development in the presence and absence of a large abundance of ferric oxide particles (Fe_2O_3) in the initial inoculum. We study how the presence of such alternative electron acceptors influences MFC startup and impacts on the resulting bioanode performance. Results are correlated to the capacity of the exo-electrogenic biofilm to carry out EET to the bioanode in the presence or absence of an alternative solid Fe_2O_3 electron acceptor.

Electrochemical characterization of the MFCs via cyclic voltammetry shows a response typical of bacterial-catalyzed acetate oxidation and EET after biofilm development in the absence of Fe_2O_3, while bio-anodes formed in the presence of Fe_2O_3 show weak or no apparent EET even after the development of a robust biofilm on the electrode surface. This inhibitory effect of solid Fe_2O_3 was found to be reversible by removing the bioanode from contact with the solid particles, suggesting a preferential use of the Fe_2O_3 by bacteria even in when present in a biofilm developed at the electrode surface. 16S rRNA amplicon sequencing of biofilms indicates a very similar community composition at both bioanode types with a large predominance of an as-yet uncultured *Pelobacter* genus. Considered together, our results suggest a possible modulation of the metabolism of exo-electrogenic biofilms in the presence of competing acceptors, which may dictate whether or not the resulting biofilm is capable of EET with the anode. Our results demonstrate the importance of considering the contribution of solid metal oxides present in the inoculum to the observed electrochemical response of exo-electrogenic biofilms.

2. Material and Methods:

2.1. *Chemicals and Materials*

NaCl (99.5%), KCl (99.5%) Sodium Acetate (>99%, anhydrous) and Glutaraldehyde (25% solution) were purchased from Sigma Aldrich and used without further purification. Ferric Oxide (Fe_2O_3, > 99%) was purchased from Fluka. Ethanol (96%) was purchased from VWR.

2.2. *Bio-anode Setup*

MFC pilots were built in a typical two compartment arrangement separated by a Proton Exchange Membrane (Fumasep® FKM). The cathodic compartment contained saline solution (10 mM NaCl) with 50 mM of potassium hexacyanoferrate III ($K_3Fe(CN)_6$) as an electron acceptor. In the second compartment 80 g of blended inoculum (garden compost, Rennes 2021) was mixed with 200 mL of saline solution in ultrapure water for a final NaCl concentration of 10 mM. This salt concentration was chosen based on previous MFC studies which successfully developed bioanodes capable of oxidising organic substrates from mixed inoculum [30]. A

graphite rod (MorganAM&T) was placed in both compartments connected through external resistance between them equivalent to the internal resistance of the set-up measured between the two electrodes; typical values of apparent internal resistances were on the order of 100 Ω as determined using electrochemical impedance spectroscopy characterisation of the full cell (Supporting Information Figure S1). Pilots with starting inoculum only were considered as 'Control' MFC pilots. For the Ferric Oxide-Enriched pilots, Fe_2O_3 powder was mixed with the blended inoculum to a final concentration of 2 g L^{-1}.

2.3. *Incubation conditions*

All pilots were incubated at a constant temperature of 25°C using a water bath. The anodic compartment was flushed regularly (every two days on average) using Ar gas to ensure anaerobic conditions. On the second day of incubation, sodium acetate was added to all pilots for a final concentration of 20 mM. Unless otherwise specified, new additions were made every 5 days on average in all pilots from anaerobic stock solutions of 0.25 µm filtered sodium acetate in ultrapure water using a sterile syringe. The pH values of the anodic medium, internal resistances and the potentials of the anodes were monitored regularly for all pilots. pH values always remained between 7.5 and 8.5 for the anolyte during the entire incubation period and were not manually adjusted. Electrochemical studies were performed under conditions of Ar saturation at regular intervals in order to follow the evolution of the bio-electrochemical profile of the anodic biofilms.

2.4. *Electrochemical studies*

Electrochemical studies were performed on a Multi Autolab/M204 potentiostat. All electrochemical studies were made using an Ag/AgCl electrode (saturated KCl, + 197 mV vs SHE) inserted into the anolyte. The bio-anode was used as the working electrode while a graphite rod mounted in the catholyte was used as a counter electrode. Fuel cell polarisation curves were obtained by applying potentials ranging from open circuit potential (OCP) *ca.* 700-800 mV to short circuit in steps of 100 mV. Each potential step was held for a minimum of 900s and the final current recorded was taken as the average of the last three data points. Power densities were obtained by multiplying current densities normalised by the geometric area of the electrode by the applied voltage ($P = j \times V$).

2.5. *DNA extraction and Amplicon sequencing*

After 54 days of incubation, the biofilms colonizing the anodic electrodes of four pilots were removed using a sterile spatula. Suspended sediments and anolyte were also collected near the electrode and a DNA extraction protocol was performed on all samples according to the manufacturer's guidelines (DNeasy PowerSoil DNA extraction kit, Qiagen®) for all samples. All biofilm and sediments samples showed satisfactory DNA concentrations as estimated using Nanodrop® hardware. 16S rRNA gene sequencing was then made on the DNA extracted from biofilm and sediments with amplification of the V4-V5 region using the primers 515F (5'-GTGCCAGCMGCCGCGGTAA-3') and 928R (5′-CCCCGYCAATTCMTTTRAGT-3') by the GeT-Biopuces laboratory of INSA Toulouse. Amplicons were then sequenced using a MiSeq Illumina® and the reads were obtained under the FastQ format.

2.6. *16S rRNA gene sequences library treatment*

The obtained 16S rRNA library in FastQ format was treated using the FROGS pipeline[31] as previously reported [32]. Briefly, this involved pre-processing sequences to cluster them in operational taxonomy units (OTUs), eliminate chimera, filter sequences with low abundance (keeping only those appearing more than 0.005% in the whole dataset) and finally, attribute the remaining OTUs left using the silva 132 16S database [33]. For all samples reported the number of sequences always exceeded 20 000, which was considered sufficient for the 16S rRNA study. The identification was stopped at the genus level and only those with a relative abundance equal or more than 4% were kept in the final analysis.

2.7. *SEM Imaging*

Bioanodes from control and ferric-oxide pilots were fixed using a 2.5% glutaraldehyde solution in 0.1M phosphate buffer overnight followed by rinsing in 0.1M phosphate buffer and dehydration in ethanol-water solutions with increasing ethanol concentration as previously reported [2]. Bioanodes were then critical-point dried to replace remaining water with CO_2 and covered in a layer of sputtered gold prior to analysis.

3. **Results**

3.1 Ferric oxide characterisation

SEM images of the Fe_2O_3 powder showed heterogeneous particles ranging between 1 – 10 µm in size (Supporting Information Figure S2). Redox processes attributable to the particles disappeared after 0.45 µm filtering of Fe_2O_3 suspensions (Supporting Information Figure S3).

No significant leaching of Fe cations was detected in solution via inductively-coupled plasma optical emission spectroscopy (ICP-OES) after incubation for >10 days under comparable conditions to those used in MFC studies (Supporting Information Figure S4) suggesting that the observed redox behaviour may be directly attributed to the couple of solid Fe_2O_3/Fe^{2+}. Presence of Fe_2O_3 at the surface of electrodes incubated in the presence of Fe_2O_3 powder was confirmed via SEM-Energy Dispersive X-Ray Spectroscopy (EDS, Figure S8).

3.1. *Effect of Ferric Oxide-Enriched Inoculum on MFC Startup*

In order to study the effect of the presence of an abundant (2g L^{-1}) solid source of Fe(III) on bioanode development, commercial ferric oxide (Fe_2O_3) microparticles were chosen to supplement natural compost inoculum in four of the MFC pilots. Four Control pilots were maintained with only compost. The effect of Fe_2O_3 presence on fuel cell startup is summarised in Figure 1. Figure 1 a) shows the average development of the open circuit potential (OCP) of pilots. OCP development under these conditions is determined

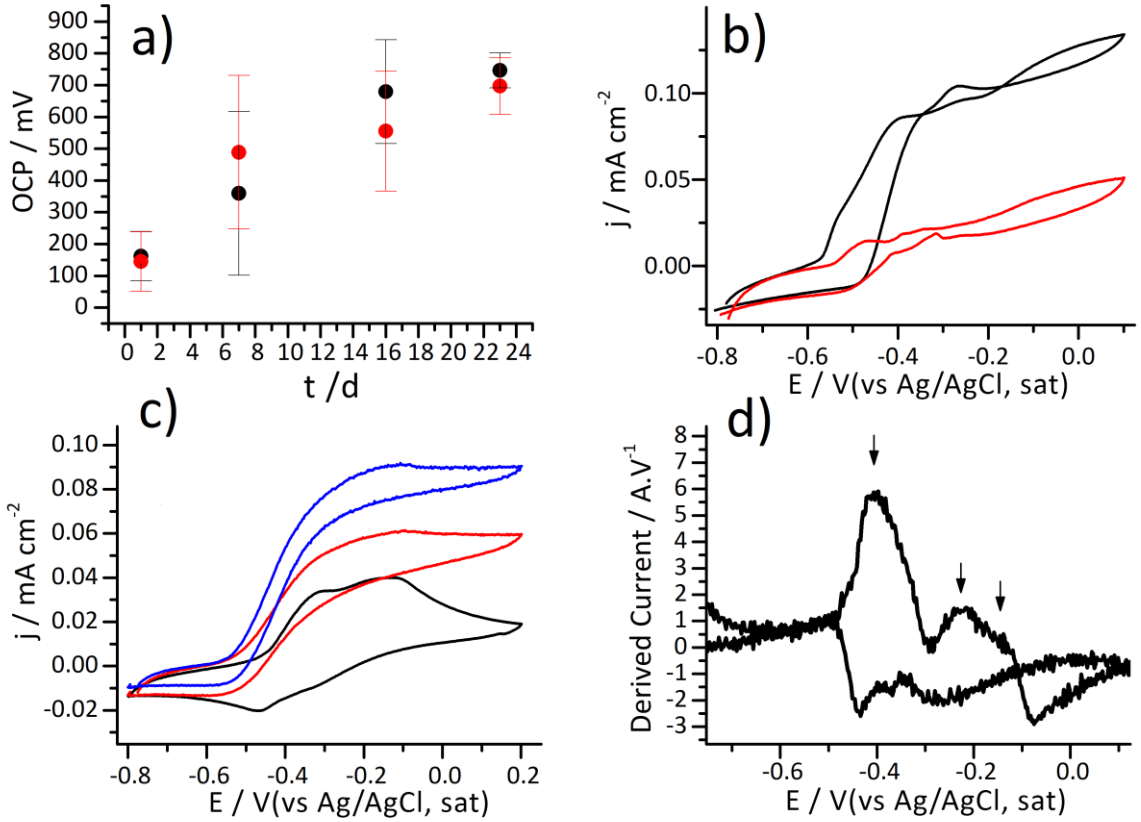

Figure 1. a) Open circuit potential values of MFC Pilots obtained with (red points) and without (black points) the presence of 2 g L^{-1} ferric oxides. b) Cyclic Voltammograms obtained on pilots with (red curve) and without (black curve) addition of 2 g L^{-1} ferric oxides after 14 days of incubation in 20 mM acetate. Both pilots had similar open circuit potentials. Scan rate: 1 mVs^{-1}. c) Cyclic voltammograms of a mature bioanode under non-turnover conditions and with successive additions of acetate to demonstrate catalytic acetate oxidation. Prior to the measurement the MFC was operated for 10 days without acetate addition. Voltammograms at a scan rate of 1 mVs^{-1} were taken 2h after each addition of sodium acetate to the anolyte from an anoxic stock solution. d) Derivative analysis of bioanode under non-turnover conditions from c). Midpoint potentials identified from the anodic scan are indicated with arrows.

versus a cathode with a constant potential *ca.* 0.2V vs Ag/AgCl (sat) due to the presence of 50 mM potassium hexacyanoferrate(III) as previously reported [2]; this potential was periodically measured and remained unchanged throughout the entire experiment, and hence the measured OCP reflects changes occurring in the bioanode over time.

The average OCP obtained at all time points was not significantly different between Ferric Oxide-enriched MFCs and controls, suggesting that pioneer exoelectrogens which oxidise acetate (*ca.* -0.488 V vs Ag/AgCl (sat)) are able to colonize the anode even in the presence of the microparticles. There is a relatively large variability in the OCP during the startup period, even between similar pilots, however upon reaching values of *ca.* 700-800 mV the OCP was continually monitored and found to remain stable in this range over time as long as periodic (once every 5 days on average) additions of sodium acetate were made from filtered, anoxic stock solutions.

However, the attainment of a particular OCP value for the MFC does not necessarily imply that the extent of colonisation by exo-electrogenic bacteria is comparable between Control and Ferric Oxide-enriched pilots. This can be seen in Figure 1 b), which compares voltammograms obtained for MFC pilots after 14 days of incubation. As evident in the figure, pilots with and without ferric oxides with similar OCP values (*ca.* 700-800 mV) nevertheless show very different extents of exo-electron colonisation as judged by their voltammetric responses. Both pilots display an onset of oxidation between -0.5 V and -0.4 V vs Ag/AgCl (sat) characteristic of organic matter oxidation by an exo-electrogenic biofilm colonizing the anode [7, 16]. Numerous peaks are observed in this potential range which may be attributed to enzymatic electron exchange due to the presence of c-type cytochromes in the biofilm. The limiting Faradaic current observed on the control pilot is *ca.* 4 times higher than when solid Fe_2O_3 particles are present, suggesting that initial bioanode development is more advanced for this pilot.

3.2. *Characterisation of mature bioanodes in absence of ferric oxide particles*

After the initial study of MFC startup the pilots were operated for at least 30 days continuously, until day-to-day measurements of the limiting current density attributed to catalytic acetate oxidation reached at least 0.1 mA cm^{-2} in the pilots without Fe_2O_3. At this point such biofilms yielded reproducible voltammograms with a sigmoidal catalytic profile consistent with a well-developed bioanode. Figure 1c) shows the electrochemical response of such a mature biofilm under non-turnover conditions; at least 3 pairs of redox peaks are identified in the voltammograms with midpoint potentials at *ca.* -0.4, -0.25 and -0.18 V vs Ag/AgCl (sat) identified via derivative analysis (Figure 1 d)). Successive additions of low concentrations of acetate returns the biofilm to turnover conditions, restoring the sigmoidal catalytic profile and confirming that the Faradaic response observed from the bioanodes is acetate-dependent. This acetate dependence was also replicated on other, independent pilots (Figure S5). Moreover, we confirmed that this catalytic response is specifically attributed to the biofilm developed at the bioanode surface by placing an unmodified graphite electrode into the anolyte of a well-developed control pilot (Figure S6). No redox peaks or catalytic acetate response were detected in these latter studies, which strongly suggests that bacteria in the biofilm are essential for harvesting electrons from acetate oxidation via extracellular electron transfer (EET).

3.3. *Characterisation of bio-anodes obtained in presence of ferric oxide particles*

The addition of ferric oxides to the starting inoculum results in key differences in the electrochemical response of mature bioanodes. Figure 2 a) and b) compares the voltammograms obtained for control and ferric oxide MFC pilots after 30 days of operation. The mature control bioanode shows more pronounced cytochrome c-like peaks in the range from -0.5 – -0.1 V vs Ag/AgCl (sat) as well as the catalytic response to acetate evident in Figure 1 b) and c). However, the bioanode developed in the ferric oxide pilots shows a very different voltammetric profile with a significantly greater apparent capacitance as well as the appearance of additional redox species with oxidation peaks in the range from -0.2 – 0 V and a broad reduction between -0.4 and -0.6 V vs Ag/AgCl (sat). We note that peaks in the range -0.5 V – -0.2 V which we attributed to the presence of c-type cytochromes in an electroactive biofilm for control pilots are also present for the ferric oxide pilot, suggesting that exo-electrogenic bacteria from the inoculum are able to colonise the electrode even in the presence of solid Fe_2O_3. This conclusion is supported by SEM images of control (Figure 2 c)) and ferric oxide (Figure 2 d)) bioanodes which show evidence of mixed biofilms present at the electrode surface. Moreover, the bioanode immersed in Fe_2O_3 was found to show evidence of bacterial colonisation predominantly by rod-shaped bacteria in direct

contact with ferric oxides (Figure 2 e) and f)). Further supporting images showing the similarities in biofilm structure for both bioanode types as well as a discussion of the chemical contribution of Fe_2O_3 particles derived from EDS data are reported in the Supporting Information in Figure S7-S12. Despite this biofilm presence, the apparent catalytic response to acetate for ferric oxide pilots is weak to non-existent even after the addition of 10 mM acetate (Supporting Information Figure S13).

Based on control experiments using graphite electrodes in direct contact with ferric oxide particles (Figure S14), we attribute the additional observed redox peaks in Figure 2 b) to oxidation and reduction of Fe_2O_3 to Fe(II) present in close proximity to the anode surface with formal potential $E^{0'}$ = -0.32 V vs Ag/AgCl (sat). This result is in good agreement with previous reports of the redox potential of the α-Fe_2O_3/Fe^{2+} couple at neutral pH [16]. Considering the formal reduction potential of acetate ($E^{0'}$= -0.49 V vs Ag/AgCl (sat) at pH 7), this demonstrates that the Fe_2O_3 particles can in principle serve as the electron acceptor for an acetate-oxidizing bioanode and may explain why Ferric Oxide-enriched pilot MFCs display no apparent acetate response despite the evident colonization of the bioanode.

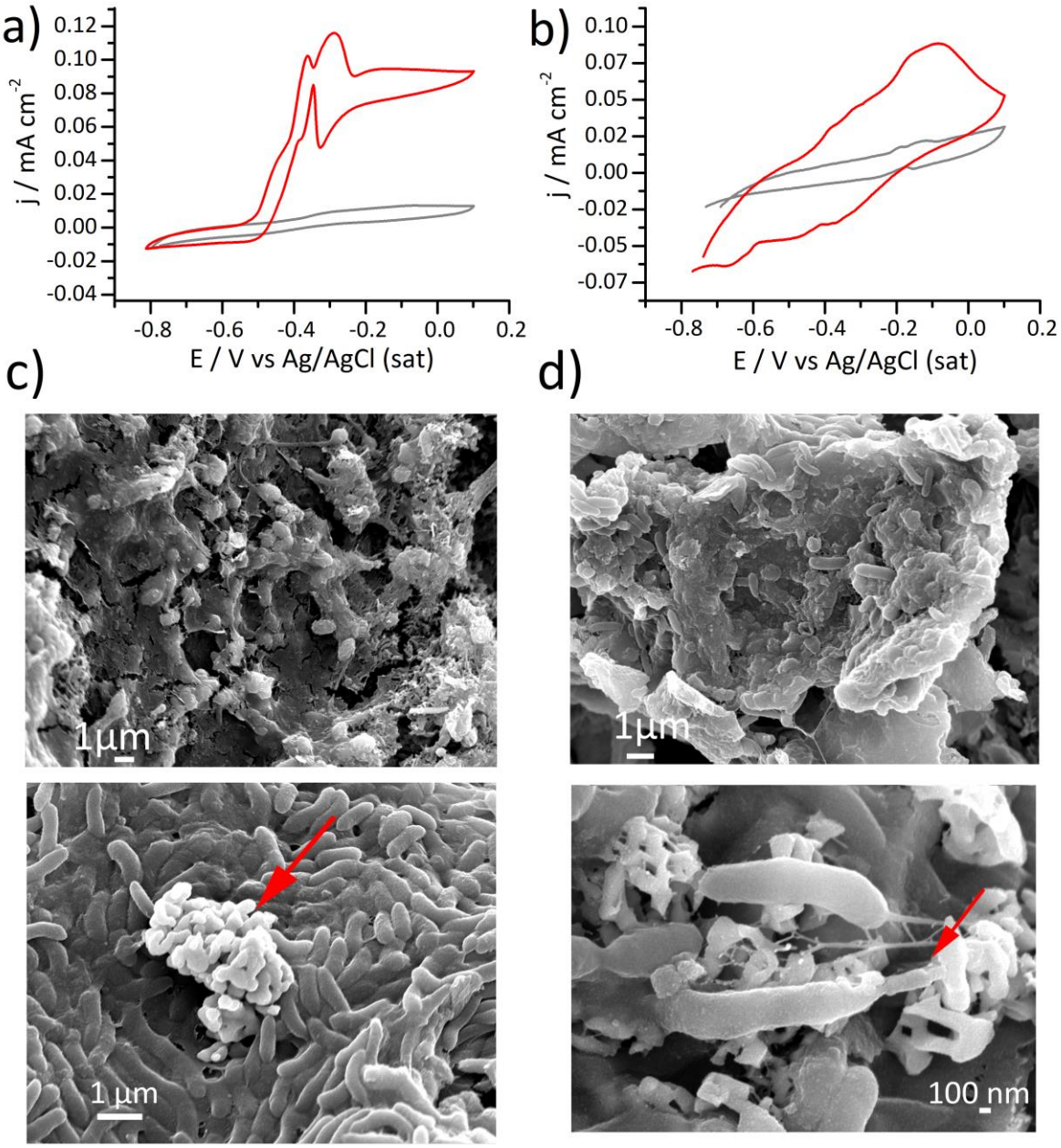

Figure 2). Typical voltammograms of bioanodes in a) Control and b) Ferric Oxide MFC pilots after 7 days (gray curve) and 30 days (red curve) of development (2nd voltammogram shown in each case). SEM images of a mature bioanode from Control (c) and Ferric Oxide pilots (d) showing mixed biofilm development. e) Direct contact between bacteria and Fe_2O_3, indicated by red arrow. f) Direct growth of individual bacteria on Fe_2O_3 particles apparently immobilised in the biofilm at the electrode surface. Apparent point of direct contact between an individual bacterium and Fe_2O_3 is indicated by the red arrow.

The extent of electrogenic biofilm development was also assessed via polarization experiments on the MFC pilots. Control pilots (Figure 3 a) and b)) and Ferric Oxide pilots (Figure 3 c) and d) were assessed on day 21. As shown in Figure 3, initial biofilm development in the absence of ferric oxides resulted in maximum power densities *ca.* 200 – 250 mW m^{-2}, with higher values of

ca. 450 mW m^{-2} obtained after 30 days of incubation (Supporting Information Figure S15). This result is comparable to previous studies of biofilm development from the group using mixed inoculum on graphite [2, 17]. By contrast, in the presence of Fe_2O_3 much lower maximum power densities of 30 – 40 mW m^{-2} were observed after similar incubation times despite the fact that pilots under both conditions have similar OCP values (between 0.7 – 0.8 V).

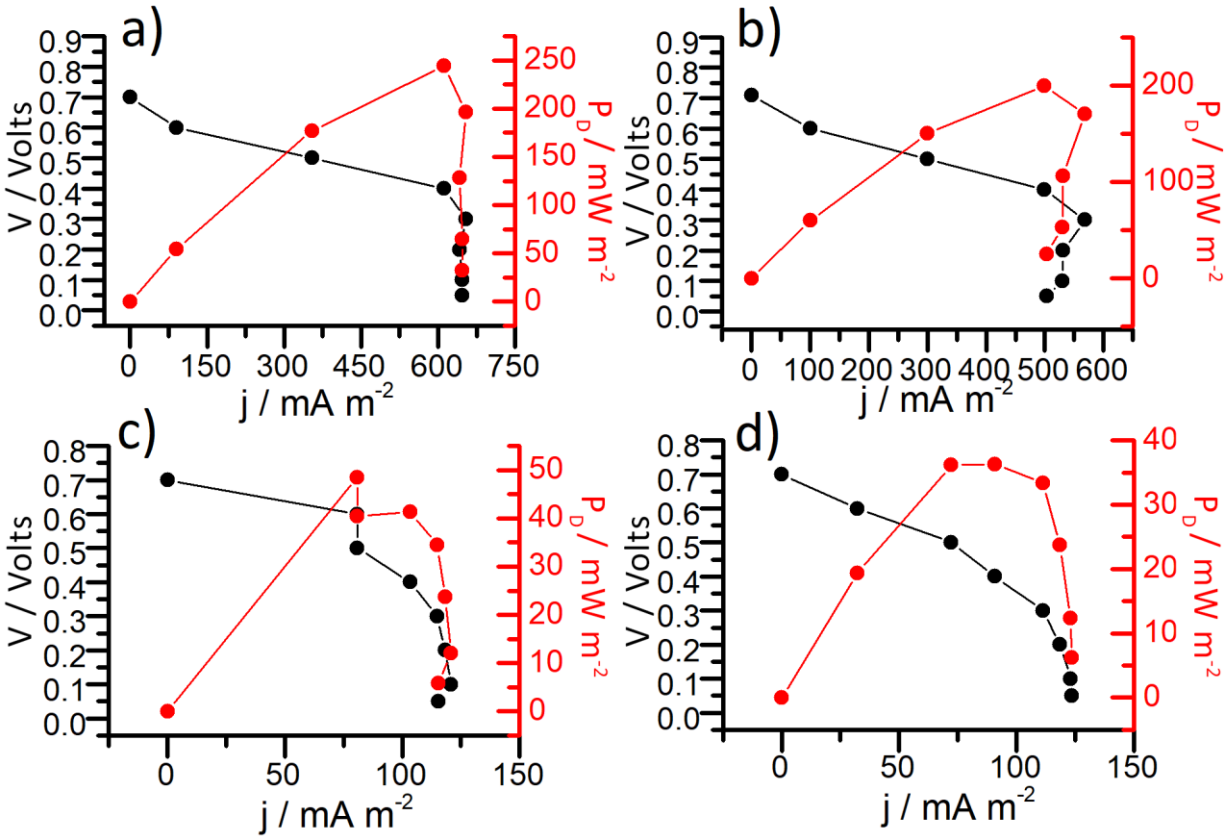

Figure 3. Fuel cell polarization curves of Control ((a) and b)) and Ferric Oxide ((c) and d)) bioanodes after 21 days of operation in 10 mM acetate/10mM NaCl under conditions of Ar saturation. The applied potential was varied from the measured open circuit potential to within 50 mV of short circuit in steps of 100 mV, as detailed in the Experimental section.

From this, as well as the confirmation of bioanode colonization from SEM images and voltammetric experiments, it may be suggested that the presence of Fe_2O_3 in the blended inoculum serves as an alternative solid electron acceptor to the anode, even when the biofilm is composed of bacteria apparently capable of EET.

3.4. *Investigation of the specific effect of ferric oxide particles on the bioanode response to acetate*

Experiments reported in Figures 1-3 suggest that the presence of solid Fe_2O_3 particles in the inoculum suppressed EET to the anode even in bioanodes with a well-developed electroactive biofilm. In order to test this hypothesis, we studied the voltammetric response of bioanodes taken

from control pilots showing EET to the anode before and after the addition of Fe_2O_3 particles. Figure 4 a shows the CV of a mature control bioanode, which showcases clear c-type cytochrome peaks as well as a catalytic acetate response with limiting current in the range of 0.1 mA cm^{-2}. After the addition of 2 g L^{-1} of ferric oxides to the anolyte an immediate drop in the limiting current of acetate oxidation to *ca.* 60% of its original value is seen (see arrow in Figure 4 a)). The bioanode under these conditions was noted to be visibly covered in a layer of Fe_2O_3 particles, similar to bioanodes obtained from incubation in Fe_2O_3 enriched inoculum (Figure S7). After incubating the bioanode in the presence of Fe_2O_3 particles for 12h overnight, the resulting voltammograms strongly resemble those of Ferric Oxide-enriched pilots from Figure 2; little apparent acetate oxidation is evident and there is a notable appearance of an additional redox peak at -0.15 V, characteristic of the presence of Fe_2O_3 particles as noted in the discussion accompanying Figure 2.

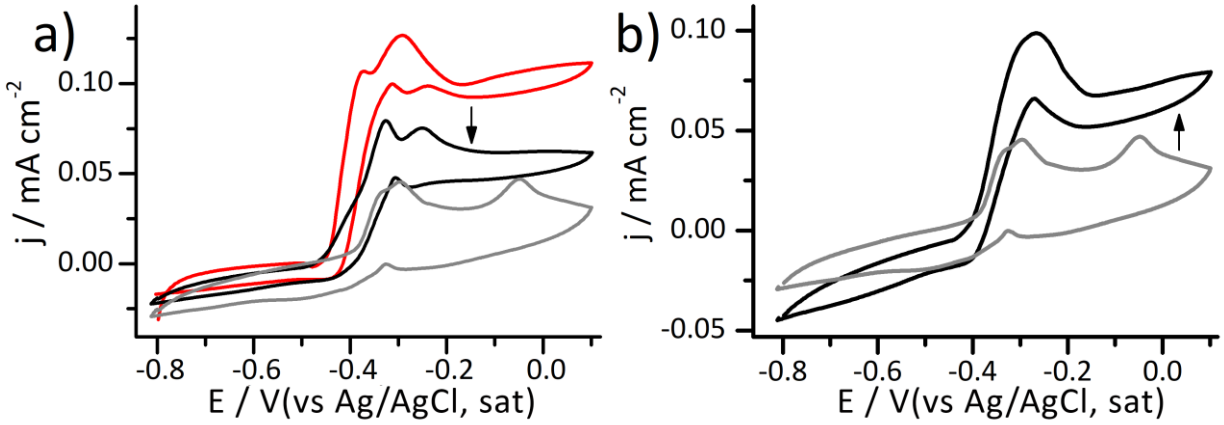

Figure 4. a) Cyclic voltammograms of a bioanode developed in a Control MFC before (red curve) and immediately after addition of solid Fe_2O_3 (black curve). The bioanode was incubated under turnover conditions in the presence of Fe_2O_3 for 12h before remeasuring the response (gray curve). b) The same bioanode described in a) before (gray curve) and after (black curve) rinsing in Ar-saturated 10 mM NaCl solution in order to remove adherent Fe_2O_3 particles and repeating the voltammetric analysis. All measurements were performed under conditions of Ar-saturation.

After gently rinsing the electrode in Ar-saturated 10 mM NaCl to detach the loosely-bound Fe_2O_3 and replacing it in fresh anolyte solution with 10 mM acetate + 10 mM NaCl, the electrode recovered its catalytic response to acetate and the peak associated with Fe_2O_3 disappeared. From this experiment we propose that exposure of our pre-existing bioanodes capable of EET to an external electrode to solid Fe_2O_3 particles suppresses EET to the anode, and this suppression can apparently be reversed by removing the affixed Fe_2O_3.

3.5. *Removal of Biofilms for 16S amplicon sequencing and community analysis*

After 54 days of operation, biofilms were removed from the graphite surface of control and ferric oxide pilots in duplicate by scraping with a sterile spatula for DNA extraction and 16S amplicon sequencing as described in the Experimental section. The removal of the biofilm at the electrode surface causes a near-total loss of the catalytic activity of the bio-anode towards acetate oxidation (Figure S16), which serves as further confirmation that the biofilm is essential for EET to the anode. For the ferric oxide pilots, biofilm removal also results in a loss of redox peaks attributed both to the biofilm itself and to adherent ferric oxide particles. We interpret this result, along with the observation of ferric oxide incorporated at the bioanode surface for Ferric Oxide pilots in SEM images (Figure 2) as a tentative confirmation that ferric oxide particles were immobilised within the developing biofilm for these MFC pilots.

3.6. *Community analysis of control and ferric oxide bioanodes*

Electrochemical results for control and ferric oxide bioanodes show a clear effect of the presence of alternative solid electron acceptors on both bioanode development and acetate oxidation. One possible explanation to observed differences between control and ferric oxide bioanodes is that the presence of ferric oxides in the inoculum alters the composition of the biofilm colonizing the anode via selective pressure effects. To test this hypothesis, we carried out community analysis through 16S amplicon sequencing of both bioanode types. Results are summarized in Figure 5.

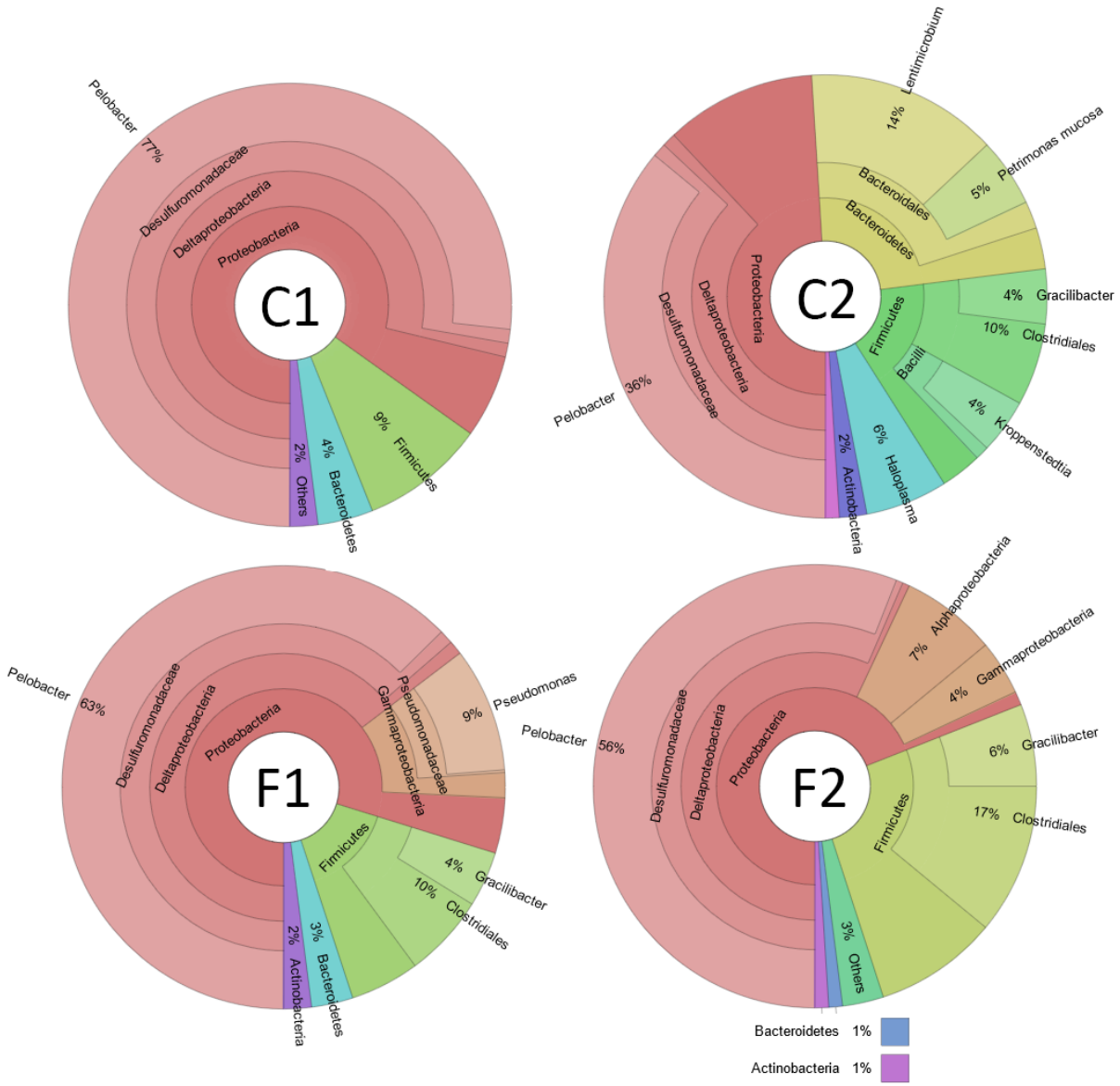

Figure 5. Details of the bacterial communities (to Genus level) colonizing the electrode from Control Pilots (C1 and C2) and Ferric Oxide Pilots (F1 and F2).

The first notable result is that for all pilots studied, there is no evidence of bacteria of well known exoelectrogens such as the *Geobacter* genus, which is perhaps the best-known acetate-metabolising electricigen used in MFC studies. Instead control pilots (C1 and C2) show a predominance of the bacterial genus *Pelobacter* with 77 % for the first pilot and 36 % in the second pilot, with ferric oxide pilots (F1 and F2) also being predominantly of the *Pelobacter* genus (63 % in F1 and 56 % in F2). Considering that this genus was only present with a very low relative abundance (<1 %) in the inoculum and surrounding milieu (community analysis of inoculum, Supporting Information Figure S17), this suggests that the incubation conditions employed during MFC startup were selective for the development of *Pelobacter*-dominated biofilms at the anode surface for both control and ferric oxide pilots. We also found no significant presence of *Pelobacter* in the surrounding anolyte milieu from samples extracted at the same

time as biofilms, suggesting that this *Pelobacter* species preferentially colonises the electrode. Bacteria in the *Pelobacter* genus have already been documented for their phylogenetical proximity with the *Geobacter* genus, both belonging to the bacterial order *Desulfuromonadales* [17]. The *Pelobacter* genus is often detected in electroactive biofilms and while it is known to contain species such as *Pelobacter carbinolicus* which are able to use solid Fe(III) oxides as an electron acceptor [28], it is generally considered incapable of both oxidising acetate and of performing EET to an electrode. Nevertheless, species of the *Pelobacter* genus do produce c-type cytochromes, which may explain the appearance of cytochrome-like redox peaks in the voltammetric analysis in Figures 1-4. [34] When blasting the OTU (Operational taxonomic unit) associated with the identified *Pelobacter* genus against the NCBI library (National Center for Biotechnology Information), the closest match is an uncultured *Pelobacter* species with only 98.3% correspondence in the sequence; blasting the same OTU against that of *Pelobacter carbinolicus*, a well-studied species of *Pelobacter* known to be incapable of EET to electrodes, yields only 95% of identity, which strongly suggests that the species colonizing our anodes is an as-of-yet unidentified species of *Pelobacter*.

4. **Discussion**

We have developed acetate-oxidising bioanodes from mixed inoculum in both the presence and absence of large concentrations of alternative solid electron acceptors in the form of Fe_2O_3. The presence of Fe_2O_3 particles results in marked differences in voltametric responses of the bioanodes, which we attribute to the suppression of EET between the biofilm and the anode in favour of insoluble Fe_2O_3 reduction.

Community analysis derived from 16S rRNA amplicon sequencing shows that the presence of Fe_2O_3 particles in the inoculum does not drive biofilm development at the anode towards radically different communities through selective pressure. Both Control and Ferric Oxide pilots show a total absence of known electricigens such as *Geobacter* or *Shewanella*, but instead have a large predominance of an as-yet unidentified *Pelobacter* species. Previous investigations of *Pelobacter* species such as *Pelobacter carbonolicus* have shown that it is capable of dissimilatory Fe(III) oxide reduction but not of direct current production on anodes; instead, a syntrophic partner such as *Geobacter sulfurreducens* must be present in order to oxidise acetate and hydrogen produced through the metabolism of ethanol by *Pelobacter* in order to produce current directly [35, 36]. By contrast, even in the absence of a known exoelectrogenic partner species, our biofilms are nevertheless capable of EET to the anode. Acetate was essential for MFC activity and all pilots were observed to show a drop in OCP and a transition to non-turnover

conditions in its absence. The presence of ferric oxide particles was found to inhibit EET, but notably, this effect could be reversed in a matter of hours when these particles were removed through gentle rinsing and the bioanodes were re-immersed in Fe_2O_3-free medium.

Based on these results, we hypothesize that all bio-anodes in this study are predominantly colonized by an as-yet unidentified *Pelobacter* species which is capable both of dissimilatory Fe(III) oxide reduction and of direct EET to a solid anode using electrons derived from acetate oxidation. To our knowledge this is the first time that EET has been demonstrated for a *Pelobacter*-colonised biofilm in the absence of a previously known exo-electrogenic syntrophic partner. The exact mechanism of EET for these biofilms has not yet been established, but direct contact of the biofilm at the anode surface was found to apparently be essential for observing EET, as no catalytic response to acetate was detected either after biofilm removal or when bare graphite electrodes were immersed in the anolyte. This suggests that direct contact EET mechanisms involving c-type cytochromes may instead be responsible for the observed currents, but does not rule out possible contributions of redox shuttles immobilised within the extracellular matrix of the biofilm [37]. Direct contact between bacteria and immobilised Fe_2O_3 was also observed for samples developed in Ferric Oxide pilots, although this does not necessarily imply a common mechanism for EET to solid metal oxides and to the bioanode. Work is currently ongoing in our laboratory to elucidate the precise origin of the observed EET for these bioanodes.

5. Conclusions

Our results demonstrate the complexity of bio-anode development under conditions of competition between potential solid terminal electron acceptors, namely Fe_2O_3 microparticles or the anode. This is of particular relevance to MFC devices developed using natural inoculum such as soils, sediments and even wastewaters, all of which may be enriched in minerals with the potential to serve as alternative electron acceptors to the anode. MFCs and other bio-electrochemical systems rely on the ability of some bacteria to perform electron transfer with solid surfaces for current generation. Here we have shown that the presence of another potential terminal electron acceptor in the incubation medium of the electrode does not necessarily preclude the species from colonizing the anode surface and becoming the predominant species in the mixed community, but can reduce the current obtained from organic matter oxidation. Further studies into the metabolic preferences of biofilms between solid surfaces and other acceptors located in the same medium are recommended in order to better understand the impact

of varied natural inocula on bio-anode development and in turn enhance the potential performance of MFC devices.

6. Declaration of Competing Interest

The authors declare that they have no known competing financial interests or personal relationships that could have appeared to influence the work reported in this paper.

7. Acknowledgement

This study was supported by the French National Research Agency (ANR-17-CE04-0004, LowNitrate and 19-CE43-0013-01, CATHOMIX). This project has received funding from the European Union's Horizon 2020 research and innovation programme under the Marie Skłodowska-Curie grant agreement No 899546. TP acknowledges the Région Bretagne for funding under grant ARED 651 NoNitrat. The authors thank the GeT-Biopuces platform of INSA Toulouse for the 16S rRNA gene sequencing study. FZAI acknowledges Université de Rennes 1 and Région Bretagne for funding under grant SAD 2076 METOX.

8. Appendix A. Supplementary data

Supplementary figures and data can be found in the attached file including determination of internal MFC resistance via impedance spectroscopy, SEM images of Fe_2O_3 particles, additional SEM and EDS analysis of biofilms, supplementary cyclic voltammetry characterization of Fe_2O_3 microparticles, supplementary MFC polarization data, SEM images of bioanodes coated with Fe_2O_3 and community analysis of inoculum and of MFC anolyte milieu following incubation,

9. References

(1) Bonanni, P. S.; Bradley, D. F.; Schrott, G. D.; Busalmen, J. P. Limitations for Current Production in *Geobacter Sulfurreducens* Biofilms. *ChemSusChem* **2013**, *6* (4), 711–720. https://doi.org/10.1002/cssc.201200671.

(2) Iannaci, A.; Myles, A.; Flinois, T.; Behan, J. A.; Barrière, F.; Scanlan, E. M.; Colavita, P. E. Tailored Glycosylated Anode Surfaces: Addressing the Exoelectrogen Bacterial Community via Functional Layers for Microbial Fuel Cell Applications. *Bioelectrochemistry* **2020**, *136*, 107621. https://doi.org/10.1016/j.bioelechem.2020.107621.

(3) Bond, D. R.; Lovley, D. R. Electricity Production by Geobacter Sulfurreducens Attached to Electrodes. *Appl. Environ. Microbiol.* **2003**, *69* (3), 1548–1555. https://doi.org/10.1128/AEM.69.3.1548-1555.2003.

(4) Bond, D. R.; Strycharz-Glaven, S. M.; Tender, L. M.; Torres, C. I. On Electron Transport through Geobacter Biofilms. *ChemSusChem* **2012**, *5* (6), 1099–1105. https://doi.org/10.1002/cssc.201100748.

(5) Commault, A. S.; Barrière, F.; Lapinsonnière, L.; Lear, G.; Bouvier, S.; Weld, R. J. Influence of Inoculum and Anode Surface Properties on the Selection of Geobacter -Dominated Biofilms. *Bioresour. Technol.* **2015**, *195*, 265–272. https://doi.org/10.1016/j.biortech.2015.06.141.

(6) Lapinsonniere, L.; Picot, M.; Poriel, C.; Barriere, F. Phenylboronic Acid Modified Anodes Promote Faster Biofilm Adhesion and Increase Microbial Fuel Cell Performances. *ELECTROANALYSIS* **2013**, *25* (3, SI), 601–605. https://doi.org/10.1002/elan.201200351.

(7) Commault, A. S.; Barriere, F.; Lapinsonniere, L.; Lear, G.; Bouvier, S.; Weld, R. J. Influence of Inoculum and Anode Surface Properties on the Selection of Geobacter-Dominated Biofilms. *Bioresour. Technol.* **2015**, *195*, 265–272. https://doi.org/10.1016/j.biortech.2015.06.141.

(8) Lovley, D. R.; Walker, D. J. Geobacter Protein Nanowires. *Front. Microbiol.* **2019**, *10*, 2078. https://doi.org/10.3389/fmicb.2019.02078.

(9) Lovley, D. R.; Ueki, T.; Zhang, T.; Malvankar, N. S.; Shrestha, P. M.; Flanagan, K. A.; Aklujkar, M.; Butler, J. E.; Giloteaux, L.; Rotaru, A.-E. Geobacter: The Microbe Electric's Physiology, Ecology, and Practical Applications. *Adv. Microb. Physiol.* **2011**, *59*, 1–100. https://doi.org/10.1016/B978-0-12-387661-4.00004-5.

(10) Logan, B. E. Exoelectrogenic Bacteria That Power Microbial Fuel Cells. *Nat. Rev. Microbiol.* **2009**, *7* (5), 375–381. https://doi.org/10.1038/nrmicro2113.

(11) Catania, C.; Karbelkar, A. A.; Furst, A. L. Engineering the Interface between Electroactive Bacteria and Electrodes. *Joule* **2021**, *5* (4), 743–747. https://doi.org/10.1016/j.joule.2021.02.001.

(12) Jiang, Y.-B.; Zhong, W.-H.; Han, C.; Deng, H. Characterization of Electricity Generated by Soil in Microbial Fuel Cells and the Isolation of Soil Source Exoelectrogenic Bacteria. *Front. Microbiol.* **2016**, *7*.

(13) Zhu, T.-T.; Cheng, Z.-H.; Yu, S.-S.; Li, W.-W.; Liu, D.-F.; Yu, H.-Q. Unexpected Role of Electron-Transfer Hub in Direct Degradation of Pollutants by Exoelectrogenic Bacteria. *Environ. Microbiol.* **2022**, *24* (4), 1838–1848. https://doi.org/10.1111/1462-2920.15939.

(14) Aelterman, P.; Rabaey, K.; Clauwaert, P.; Verstraete, W. Microbial Fuel Cells for Wastewater Treatment. *Water Sci. Technol.* **2006**, *54* (8), 9–15. https://doi.org/10.2166/wst.2006.702.

(15) He, L.; Du, P.; Chen, Y.; Lu, H.; Cheng, X.; Chang, B.; Wang, Z. Advances in Microbial Fuel Cells for Wastewater Treatment. *Renew. Sustain. Energy Rev.* **2017**, *71*, 388–403. https://doi.org/10.1016/j.rser.2016.12.069.

(16) Thomas, Y. R. J.; Picot, M.; Carer, A.; Berder, O.; Sentieys, O.; Barriere, F. A Single Sediment-Microbial Fuel Cell Powering a Wireless Telecommunication System. *J. POWER SOURCES* **2013**, *241*, 703–708. https://doi.org/10.1016/j.jpowsour.2013.05.016.

(17) Iannaci, A.; Myles, A.; Philippon, T.; Barriere, F.; Scanlan, E. M.; Colavita, P. E. Controlling the Carbon-Bio Interface via Glycan Functional Adlayers for Applications in Microbial Fuel Cell Bioanodes. *MOLECULES* **2021**, *26* (16). https://doi.org/10.3390/molecules26164755.

(18) Picot, M.; Lapinsonnière, L.; Rothballer, M.; Barrière, F. Graphite Anode Surface Modification with Controlled Reduction of Specific Aryl Diazonium Salts for Improved Microbial Fuel Cells Power Output. *Biosens. Bioelectron.* **2011**, *28* (1), 181–188. https://doi.org/10/cjsncn.

(19) Guo, K.; Freguia, S.; Dennis, P. G.; Chen, X.; Donose, B. C.; Keller, J.; Gooding, J. J.; Rabaey, K. Effects of Surface Charge and Hydrophobicity on Anodic Biofilm Formation, Community Composition, and Current Generation in Bioelectrochemical Systems. *Environ. Sci. Technol.* **2013**, *47* (13), 7563–7570. https://doi.org/10.1021/es400901u.

(20) Smida, H.; Lebegue, E.; Bergamini, J.-F.; Barriere, F.; Lagrost, C. Reductive Electrografting of in Situ Produced Diazopyridinium Cations: Tailoring the Interface between Carbon Electrodes and Electroactive Bacterial Films. *BIOELECTROCHEMISTRY* **2018**, *120*, 157–165. https://doi.org/10.1016/j.bioelechem.2017.12.006.

(21) Kiely, P. D.; Rader, G.; Regan, J. M.; Logan, B. E. Long-Term Cathode Performance and the Microbial Communities That Develop in Microbial Fuel Cells Fed Different Fermentation Endproducts. *Bioresour. Technol.* **2011**, *102* (1), 361–366. https://doi.org/10.1016/j.biortech.2010.05.017.

(22) Kiely, P. D.; Cusick, R.; Call, D. F.; Selembo, P. A.; Regan, J. M.; Logan, B. E. Anode Microbial Communities Produced by Changing from Microbial Fuel Cell to Microbial Electrolysis Cell Operation Using Two Different Wastewaters. *Bioresour. Technol.* **2011**, *102* (1), 388–394. https://doi.org/10.1016/j.biortech.2010.05.019.

(23) Katuri, K. P.; Kavanagh, P.; Rengaraj, S.; Leech, D. Geobacter Sulfurreducens Biofilms Developed under Different Growth Conditions on Glassy Carbon Electrodes: Insights Using Cyclic Voltammetry. *Chem. Commun.* **2010**, *46* (26), 4758. https://doi.org/10/ddxg5d.

(24) Jana, P. S.; Katuri, K.; Kavanagh, P.; Kumar, A.; Leech, D. Charge Transport in Films of Geobacter Sulfurreducens on Graphite Electrodes as a Function of Film Thickness. *Phys. Chem. Chem. Phys.* **2014**, *16* (19), 9039–9046. https://doi.org/10.1039/C4CP01023J.

(25) Wang, F.; Chan, C. H.; Suciu, V.; Mustafa, K.; Ammend, M.; Si, D.; Hochbaum, A. I.; Egelman, E. H.; Bond, D. R. Structure of Geobacter OmcZ Filaments Suggests Extracellular Cytochrome Polymers Evolved Independently Multiple Times. *eLife* **2022**, *11*, e81551. https://doi.org/10.7554/eLife.81551.

(26) Ren, G.; Yan, Y.; Nie, Y.; Lu, A.; Wu, X.; Li, Y.; Wang, C.; Ding, H. Natural Extracellular Electron Transfer Between Semiconducting Minerals and Electroactive Bacterial Communities Occurred on the Rock Varnish. *Front. Microbiol.* **2019**, *10*, 293. https://doi.org/10.3389/fmicb.2019.00293.

(27) Hartshorne, R. S.; Reardon, C. L.; Ross, D.; Nuester, J.; Clarke, T. A.; Gates, A. J.; Mills, P. C.; Fredrickson, J. K.; Zachara, J. M.; Shi, L.; Beliaev, A. S.; Marshall, M. J.; Tien, M.; Brantley, S.; Butt, J. N.; Richardson, D. J. Characterization of an Electron Conduit between Bacteria and the Extracellular Environment. *Proc. Natl. Acad. Sci.* **2009**, *106* (52), 22169–22174. https://doi.org/10.1073/pnas.0900086106.

(28) Richter, H.; Lanthier, M.; Nevin, K. P.; Lovley, D. R. Lack of Electricity Production by *Pelobacter Carbinolicus* Indicates That the Capacity for Fe(III) Oxide Reduction Does Not Necessarily Confer Electron Transfer Ability to Fuel Cell Anodes. *Appl. Environ. Microbiol.* **2007**, *73* (16), 5347–5353. https://doi.org/10.1128/AEM.00804-07.

(29) Li, T.; Zhou, Q.; Zhou, L.; Yan, Y.; Liao, C.; Wan, L.; An, J.; Li, N.; Wang, X. Acetate Limitation Selects Geobacter from Mixed Inoculum and Reduces Polysaccharide in Electroactive Biofilm. *Water Res.* **2020**, *177*, 115776. https://doi.org/10.1016/j.watres.2020.115776.

(30) Schaetzle, O.; Barrière, F.; Schröder, U. An Improved Microbial Fuel Cell with Laccase as the Oxygen Reduction Catalyst. *Energy Environ. Sci.* **2008**, *2* (1), 96–99. https://doi.org/10.1039/B815331K.

(31) Escudié, F.; Auer, L.; Bernard, M.; Mariadassou, M.; Cauquil, L.; Vidal, K.; Maman, S.; Hernandez-Raquet, G.; Combes, S.; Pascal, G. FROGS: Find, Rapidly, OTUs with Galaxy Solution. *Bioinformatics* **2018**, *34* (8), 1287–1294. https://doi.org/10.1093/bioinformatics/btx791.

(32) Philippon, T.; Tian, J.; Bureau, C.; Chaumont, C.; Midoux, C.; TOURNEBIZE, J.; Bouchez, T.; Barrière, F. Denitrifying Bio-Cathodes Developed from Constructed Wetland Sediments Exhibit Electroactive Nitrate Reducing Biofilms Dominated by the Genera Azoarcus and Pontibacter. *Bioelectrochemistry*, 2021, *140*, 107819.

(33) Quast, C.; Pruesse, E.; Yilmaz, P.; Gerken, J.; Schweer, T.; Yarza, P.; Peplies, J.; Glöckner, F. O. The SILVA Ribosomal RNA Gene Database Project: Improved Data Processing and Web-Based Tools. *Nucleic Acids Res.* **2013**, *41* (D1), D590–D596. https://doi.org/10.1093/nar/gks1219.

(34) Aklujkar, M.; Haveman, S. A.; DiDonato, R.; Chertkov, O.; Han, C. S.; Land, M. L.; Brown, P.; Lovley, D. R. The Genome of Pelobacter Carbinolicus Reveals Surprising Metabolic Capabilities and Physiological Features. *BMC Genomics* **2012**, *13* (1), 690. https://doi.org/10.1186/1471-2164-13-690.

(35) Rotaru, A.-E.; Shrestha, P. M.; Liu, F.; Ueki, T.; Nevin, K.; Summers, Z. M.; Lovley, D. R. Interspecies Electron Transfer via Hydrogen and Formate Rather than Direct Electrical Connections in Cocultures of Pelobacter Carbinolicus and Geobacter Sulfurreducens. *Appl. Environ. Microbiol.* **2012**, *78* (21), 7645–7651. https://doi.org/10.1128/AEM.01946-12.

(36) Kimura, Z.; Okabe, S. Acetate Oxidation by Syntrophic Association between Geobacter Sulfurreducens and a Hydrogen-Utilizing Exoelectrogen. *ISME J.* **2013**, *7* (8), 1472–1482. https://doi.org/10.1038/ismej.2013.40.

(37) Doyle, L. E.; Marsili, E. Weak Electricigens: A New Avenue for Bioelectrochemical Research. *Bioresour. Technol.* **2018**, *258*, 354–364. https://doi.org/10.1016/j.biortech.2018.02.073.

Supporting Information for: Fe(III) oxide microparticles modulate extracellular electron transfer in anodic biofilms dominated by bacteria of the *Pelobacter* genus.

Timothé Philippon, Fatima-Zahra Ait-Itto, Alicia Monfort, Frédéric Barrière,* James A. Behan*

Université de Rennes, CNRS, Institut des Sciences Chimiques de Rennes, France

**Corresponding authors: james.behan@univ-rennes1.fr*

frederic.barriere@univ-rennes1.fr

Table of Contents

Determination of Internal Resistance of Microbial Fuel Cells via Impedance Spectroscopy

To determine the apparent internal resistance of the MFC pilots, electrochemical impedance spectroscopy (EIS) experiments were carried out using the bioanode as the working electrode and the cathode as the counter and reference electrode. Measurements were carried out at OCP with an equilibration time of 600 s prior to the initiation of the EIS experiment. Data were acquired in the frequency range from 200 kHz to 10 mHz using an AC voltage amplitude of 10 mV. A typical Nyquist plot obtained under such conditions is shown in Figure S1. Here the apparent uncompensated resistance due to the solution and the cation exchange membrane of the MFC was estimated from the intercept of the data with the X-axis at 110 Ω.

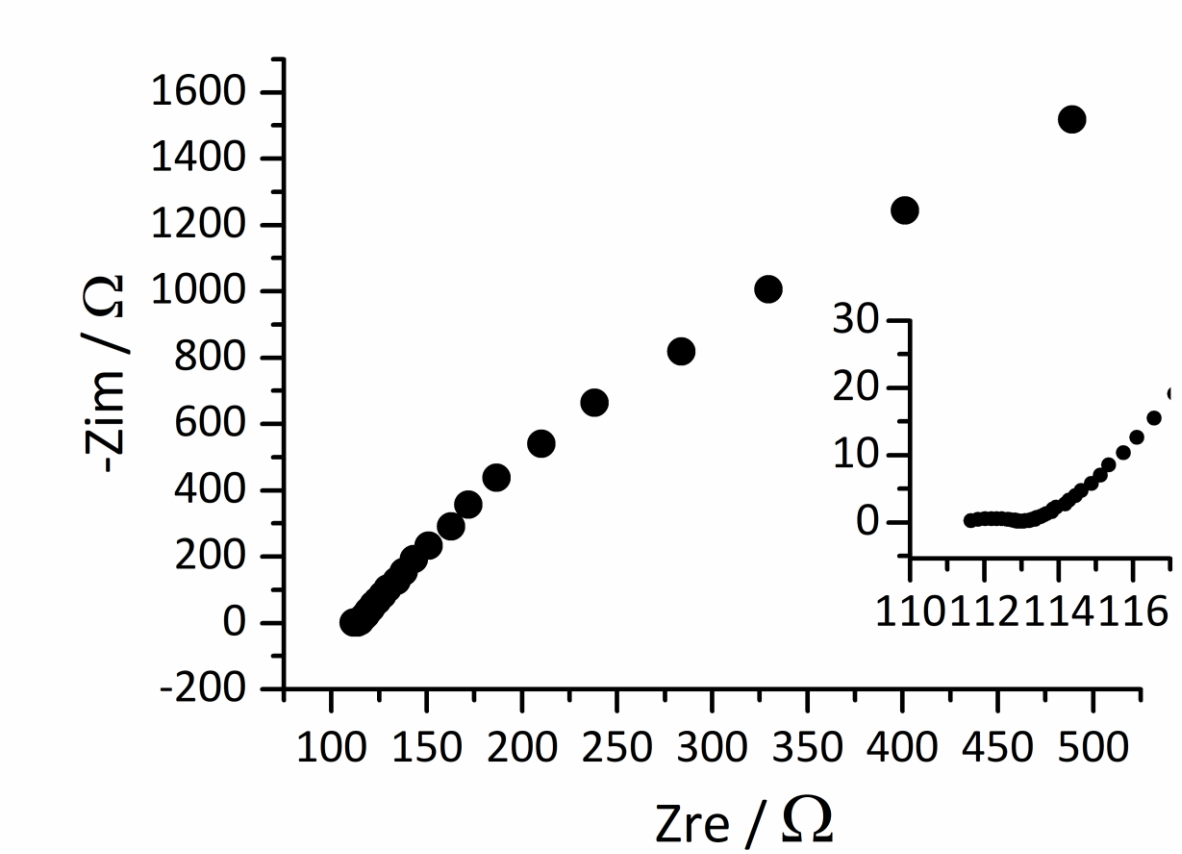

Figure S1. Representative Nyquist Plot of H-Type Fuel Cells immediately after setup.

SEM Characterisation of Fe_2O_3 Particles

Commercial Fe_2O_3 particles (Figure S2 a)) were sputter-coated with Au prior to SEM analysis. Representative images are shown in Figure S2 b) – d) at different scales. Particles are heterogeneous with the smallest apparent particles being on the order of 1 µm.

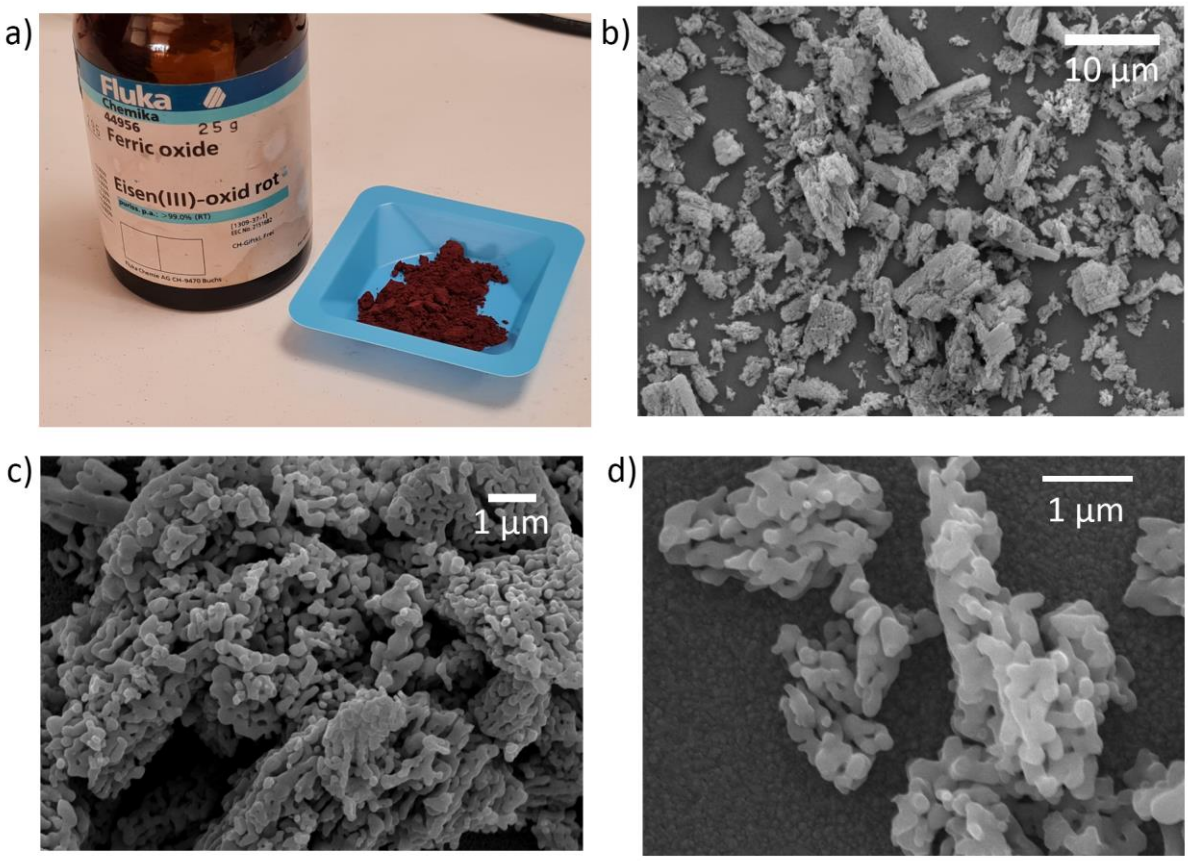

Figure S2. a) Commercial Ferric oxide (Fe_2O_3) particles used in this study b)-d) Representative SEM images of ferric oxide particles obtained at different magnifications.

Voltammetric Analysis of Fe_2O_3 Particles

Fe_2O_3 (2 g/L in NaCl 10 mM) was analyzed by cyclic voltammetry in the range -1.0 – 1.0 V vs Ag/AgCl (sat). Figure S3 shows the resulting CV curves for bare graphite in NaCl only (black trace) and after Fe_2O_3 addition (red trace). Afterwards the electrode was thoroughly rinsed with ultrapure water and the electrolyte filtered with 0.45 µm syringe filters. The resulting CV curves resemble the bare graphite electrode, suggesting that the redox species with a broad oxidation between -0.4 – 0.1 V and a reduction onset at -0.6 V vs Ag/AgCl (sat) can be attributed to the Fe_2O_3 particles.

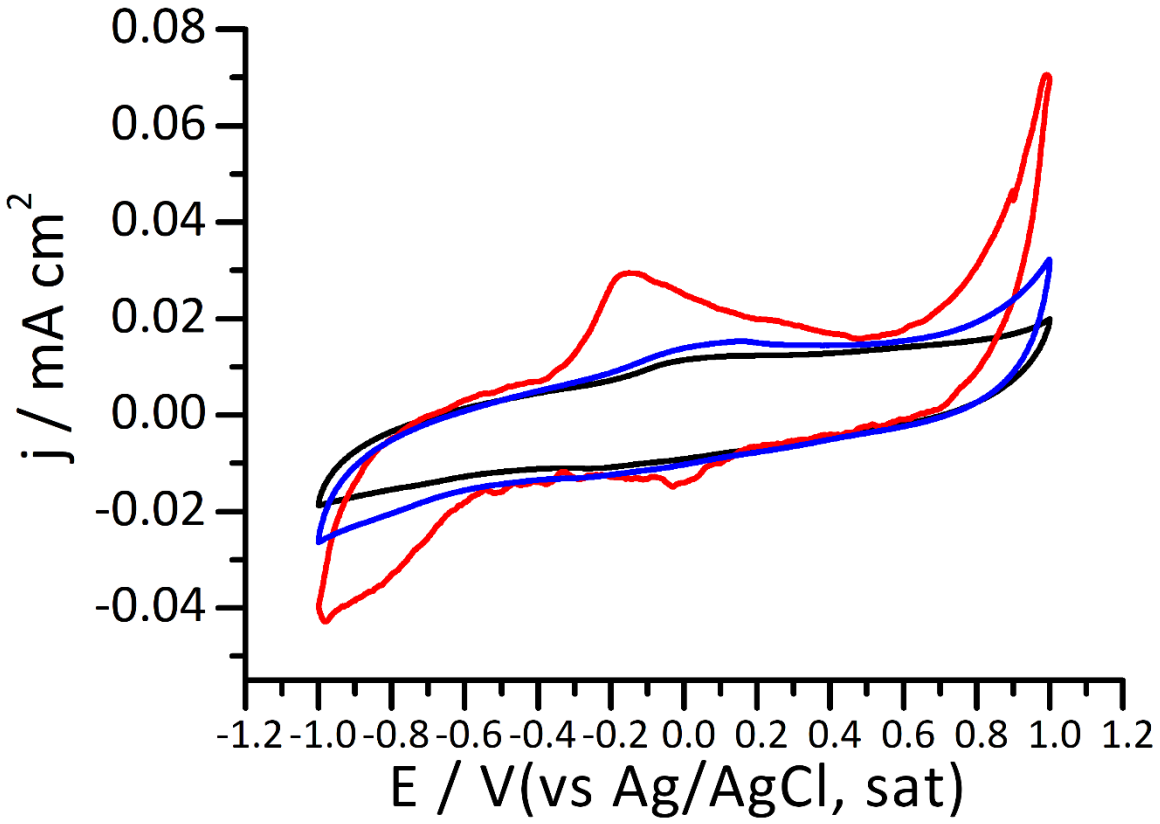

Figure S3. Cyclic voltammograms of a graphite electrode in 10 mM NaCl in the presence of 2 g L^{-1} Fe_2O_3 (red trace) and after 0.45 µm filtration to remove solid particles (blue trace). The bare graphite electrode in 10 mM NaCl only is shown in black.

Leaching Test of Fe_2O_3 Particles

To investigate the capacity of Fe_2O_3 particles to leach Fe cations into solution, Fe_2O_3 particles (2g/L) were placed in an Ar-saturated solution of 10 mM NaCl and 10 mM sodium acetate (pH = 7.3) and incubated at 30 °C. Samples were taken after 4 and 10 days of incubation, diluted with 2% nitric acid (HNO_3, analytical grade 70%, Merck) and 0.25 µm filtered prior to Inductively Coupled Plasma-Optical Emission Spectrometry (ICP-OES) analysis (iCAP 7000Series Thermo Scientific). Calibrated solutions in the range 1 – 10 mg/L Fe were prepared using commercial stock solutions of Fe and the samples were titrated for Fe under argon flux. As shown in Figure S4, detected Fe in the filtrate was

< 0.1 mg/L even after 10 days of incubation, suggesting that leaching of free Fe cations into solution is negligible under the experimental conditions employed in MFC studies.

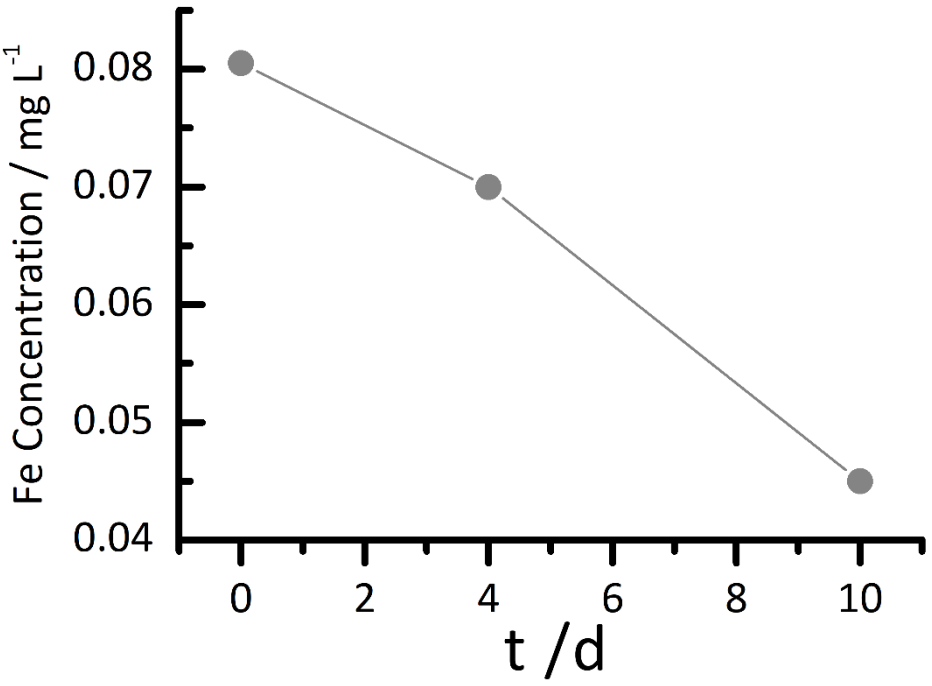

Figure S4. Free Fe ion concentration obtained from filtered solutions of 2 g L^{-1} Fe_2O_3 in 10 mM NaCl/Acetate over time via Inductively Coupled Plasma-Optical Emission Spectrometry.

Reproducibility of Acetate Response of Control Bioanodes

Replicates of the acetate response test on Control MFC bioanodes are presented in Figure S5 after a) 5 days and b) 10 days without acetate addition. Both pilots showcase a voltammogram typical of catalytic acetate oxidation. The bioanode in a) did not fully deplete acetate from the previous addition of 10 mM acetate within the 5-day period, while in b) the bioanode is closer to non-turnover conditions similar to the result of Figure 1 c) in the main text.

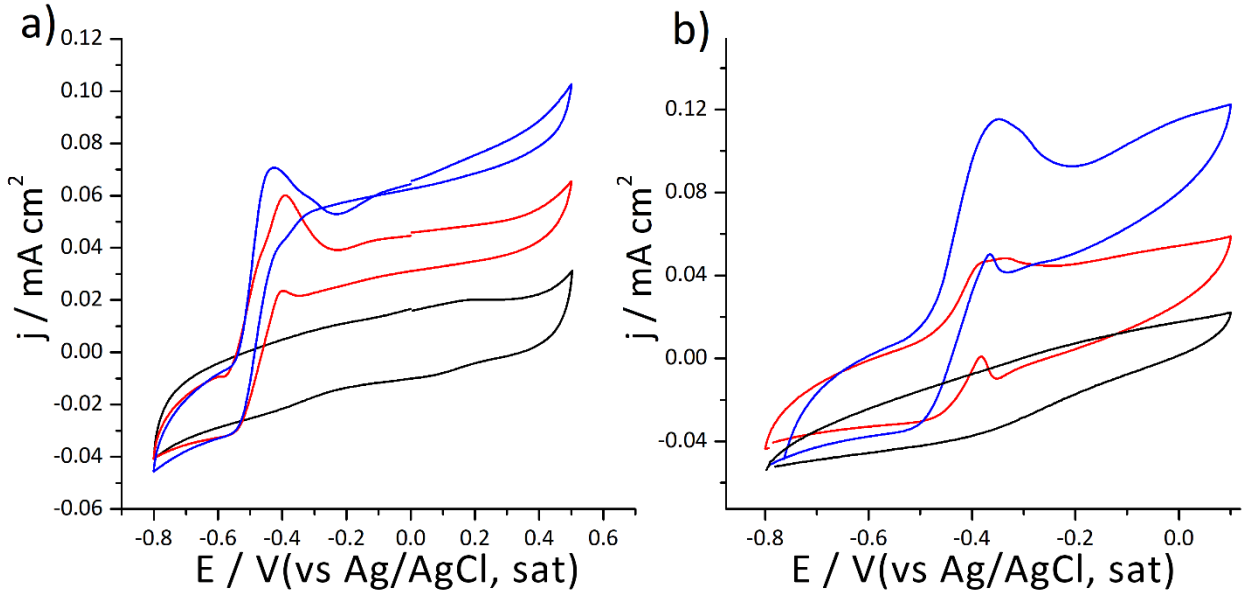

Figure S5. Replicates of the response of two independent Control bioanodes before (red trace) and after the addition of 10 mM acetate (blue trace). The black trace indicates the initial voltammograms obtained on bare graphite electrodes on day 1 of incubation.

Comparison of mature bioanodes to bare graphite electrodes in MFC anolyte after more than 30 days of incubation.

As described in the main text, mature bioanodes in Control MFCs display a characteristic acetate oxidation with a limiting current density of *ca.* 0.1 mA.cm^{-2} (red trace in Figure S6). However it is well known that bacteria in the surrounding anolyte may also be electricigens capable of extracellular electron transfer via intermediate redox shuttles. To demonstrate that the biofilm developed at the electrode surface is necessary for extracellular electron transfer (EET), the response of mature bioanodes was compared to that of bare graphite immersed in the same anolyte solution. In Figure S6 the bioanode response was first measured (red trace) before being transferred under Ar flow to an anoxic solution of 10 mM NaCl. A bare graphite electrode was then placed into the anolyte compartment and its voltammetric response recorded (black trace in Figure S6). No evidence of redox species or catalytic acetate response is detected for bare graphite, which strongly indicates that bacteria present in the biofilm are essential for the observed EET.

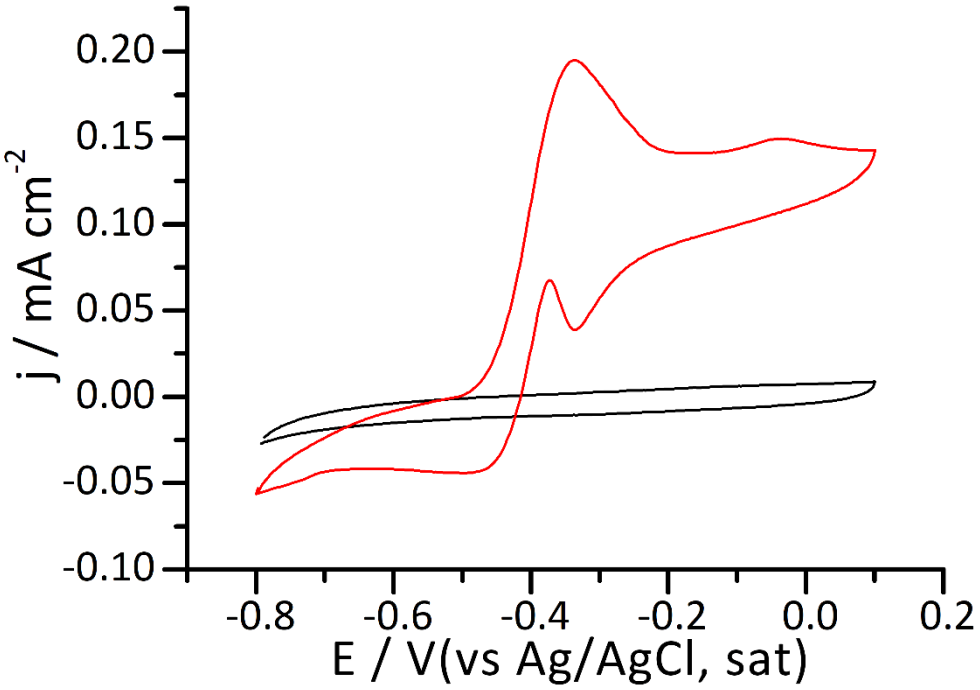

Figure S6. Cyclic voltammograms (2nd scan shown) of a mature bioanode (red trace) and bare graphite electrode (black trace) immersed in the anodic compartment of the same Control MFC pilot. Voltammograms were measured under conditions of Ar saturation after the addition of 10 mM acetate to the anolyte.

Photographs of Ferric Oxide Bioanodes After Incubation

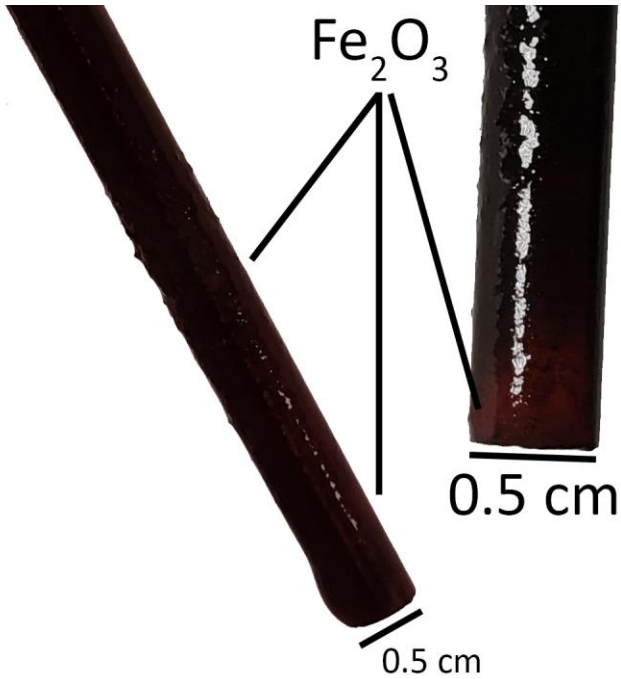

Figure S7. Photographs of Ferric Oxide Bioanodes after 50 days of incubation showing adherent Fe_2O_3 particles, as later confirmed by SEM analysis (see Figure S8-S11 below and Figure 2 in the main text).

Biofilm Composition Study through Energy Dispersive X-Ray Spectroscopy and SEM Images of Bioanodes

As discussed in Figure 2 c)-f) in the main text, mixed biofilms were identified on graphite bioanodes in both the presence and absence of adherent Fe_2O_3 at the bioanode surface. Figure S8 shows energy dispersive x-ray spectroscopy (EDS) results for bioanodes in the absence (a)) and presence (b)-d) of Fe_2O_3. Peaks associated to Fe are identified only in regions containing apparent Fe_2O_3 particles with similar morphology and size distribution to those identified in Figure S2, while control bioanodes show peaks only of carbon and oxygen, consistent with an organic biofilm.

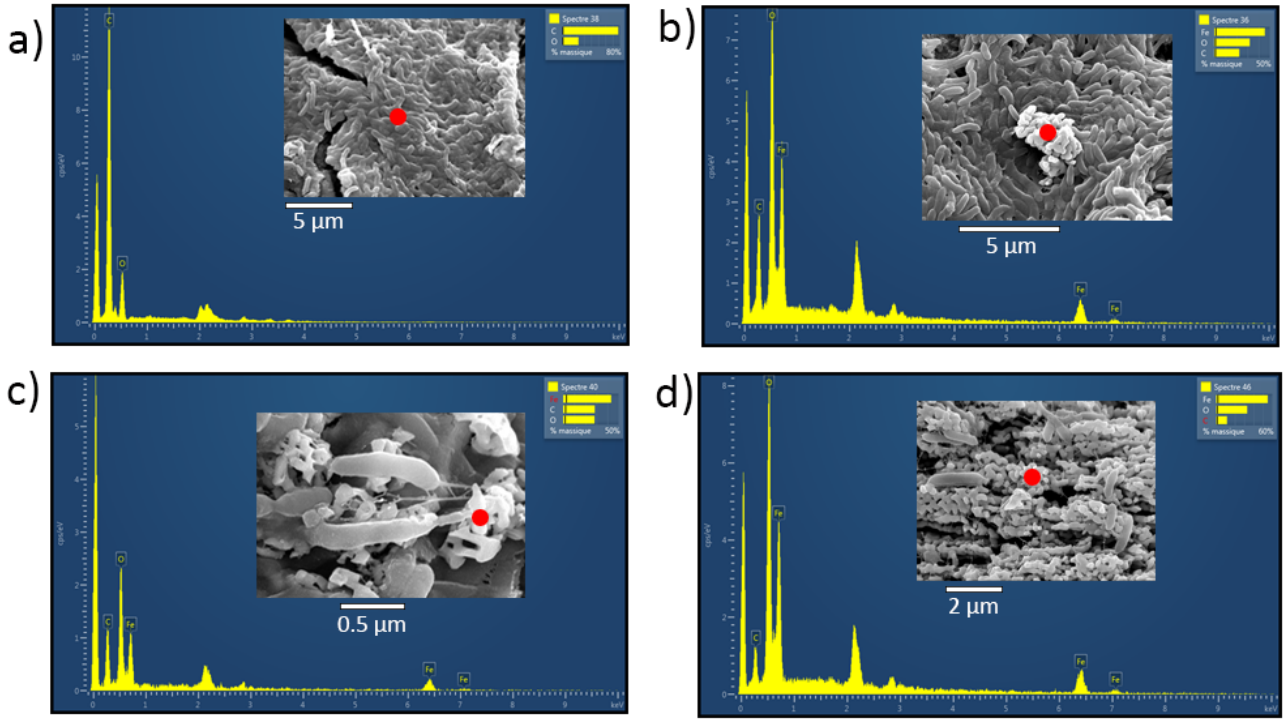

Figure S8. EDS analysis of SEM images of a) bacterial biofilm and b-d) bacterial biofilm developed on a bioanode in the presence of 2 g/L Fe_2O_3. The red spot in each image indicates the area of analysis. The unaltered images in Figure S8 are presented below.

It is clear from the accompanying images in Figure S8 (reproduced without alteration in Figure S9-S12 below) that the biofilms develop coherently across the graphite surface regardless of the presence of Fe_2O_3. Adherent Fe_2O_3 particles may attach to the biofilm as shown in Figure S8 b)-d), and individual bacteria appear to grow in direct contact with these particles (most evident in Figure S8 d) and Figure S12)). This suggests that Fe_2O_3 does not impede colonization of the bioanode by electroactive bacteria and that differences observed in the electrochemical response of control and Fe_2O_3 bioanodes should instead be attributed to the presence of an alternative terminal electron acceptor to the anode.

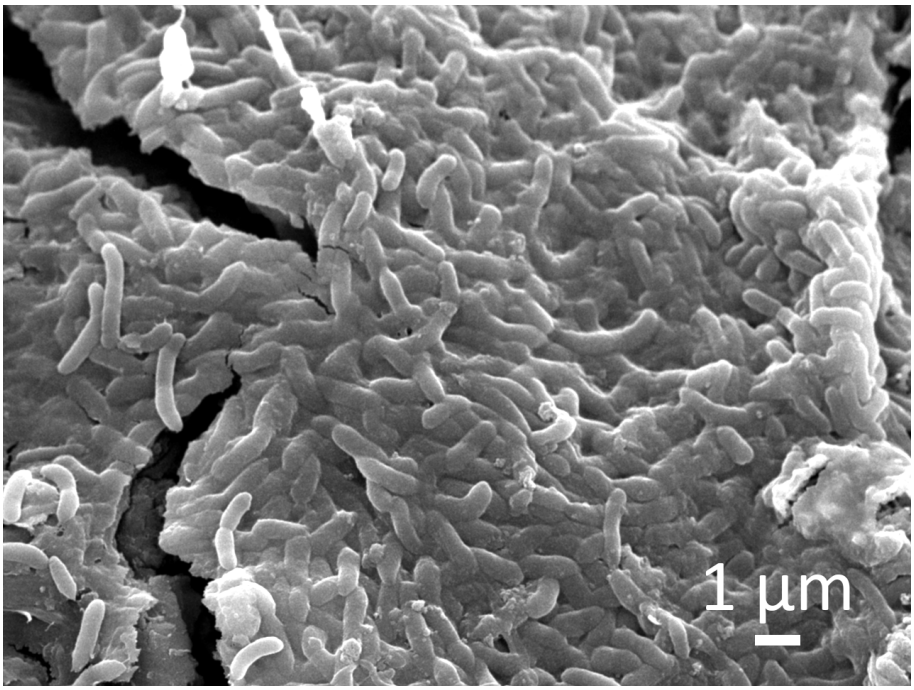

Figure S9. Bacterial biofilm from bioanode identified in Figure S8 a).

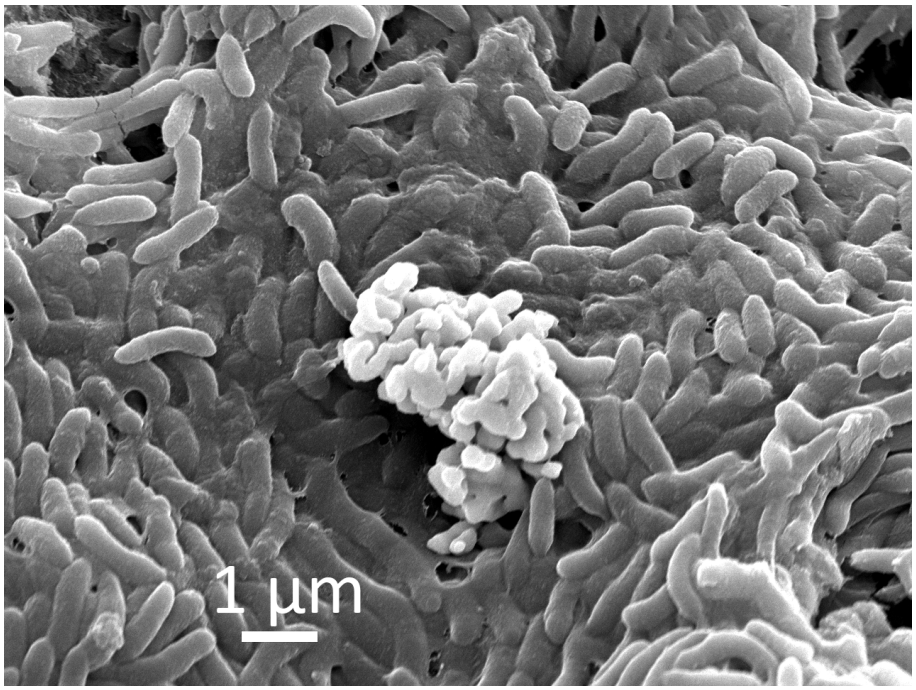

Figure S10. Biofilm developed in the presence of Fe_2O_3 particles from Figure S8 b). This image was also presented as Figure 2 e) in the main text.

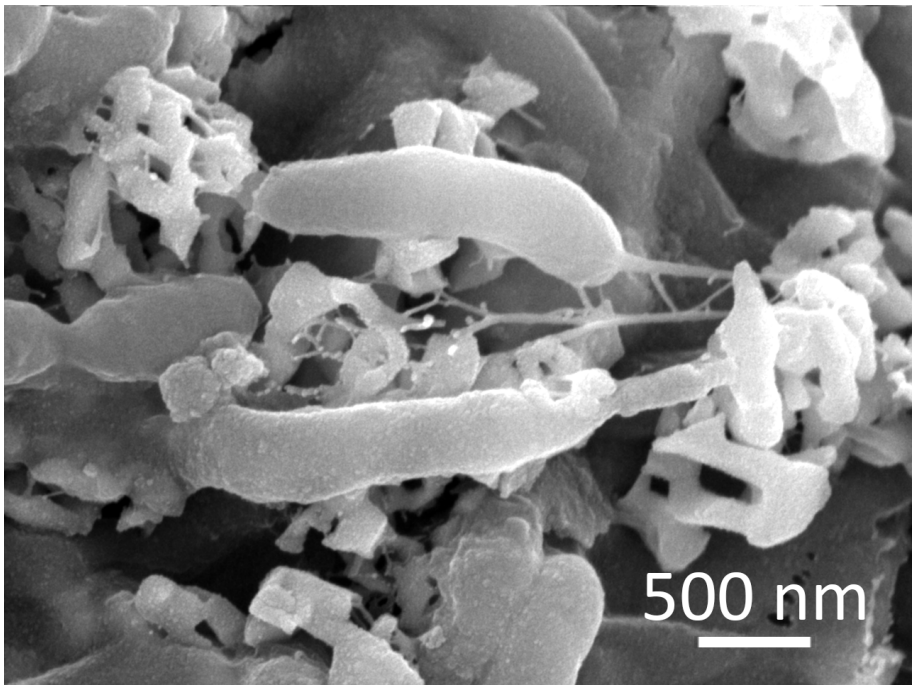

Figure S11. Bacteria developing at graphite electrode surface in contact with Fe_2O_3 particles from Figure S8 c). This figure was also presented as Figure 2 f) in the main text.

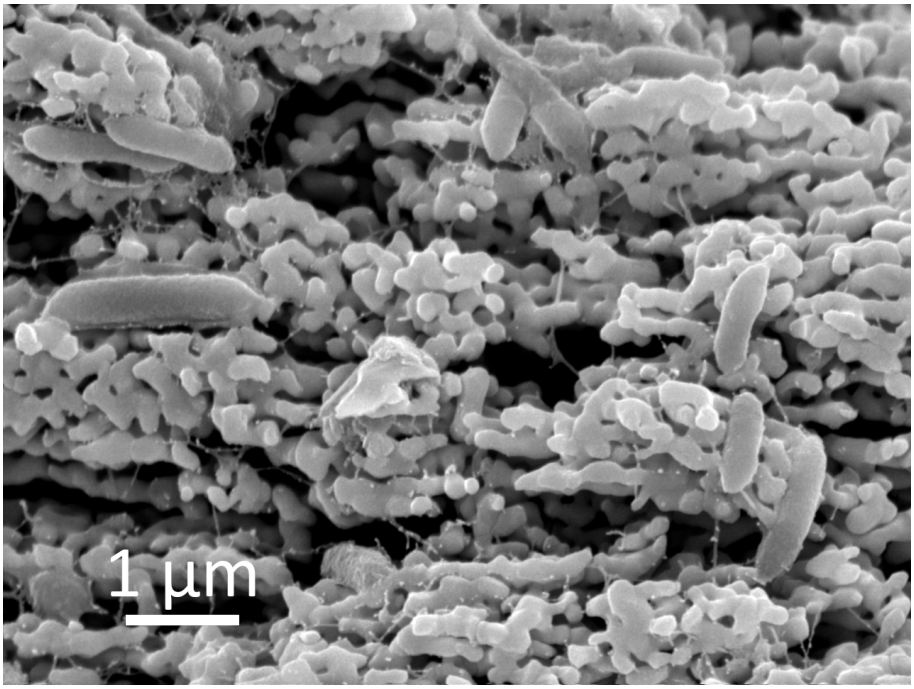

Figure S12. Images of bacteria growing on a graphite electrode covered in adherent Fe_2O_3 particles from Figure S8 d). Multiple bacteria are evident in the figure as well as protruding pili apparently connecting the bacteria to the Fe_2O_3 modified electrode.

Lack of Acetate Response Evident in Voltammograms of a Ferric Oxide bioanode

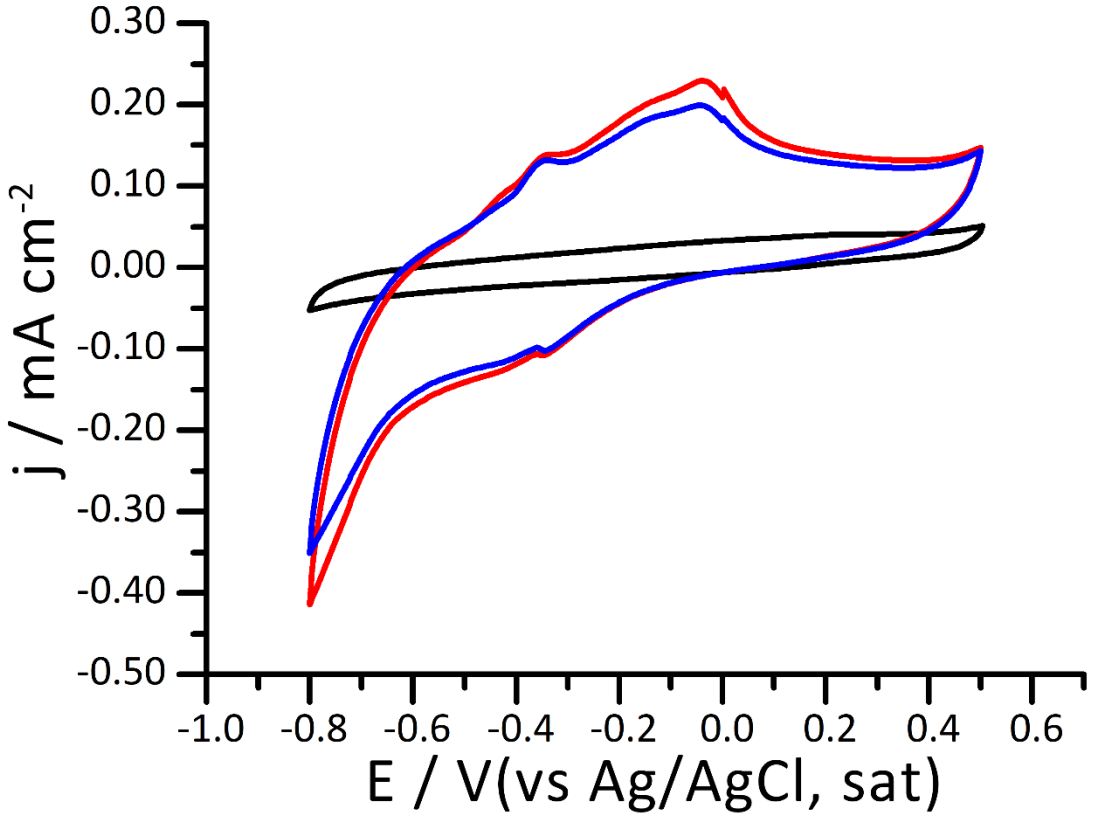

Figure S13. Voltammograms of a Ferric Oxide bioanode before (blue curve) and after (red curve) addition of 10 mM sodium acetate. The black curve shows the initial voltammogram obtained for bare graphite. Unlike for Control bioanodes, very little change is evident in the voltammogram after acetate addition.

Additional Voltammetric Characterisation of Fe_2O_3 particles in direct contact with graphite electrodes

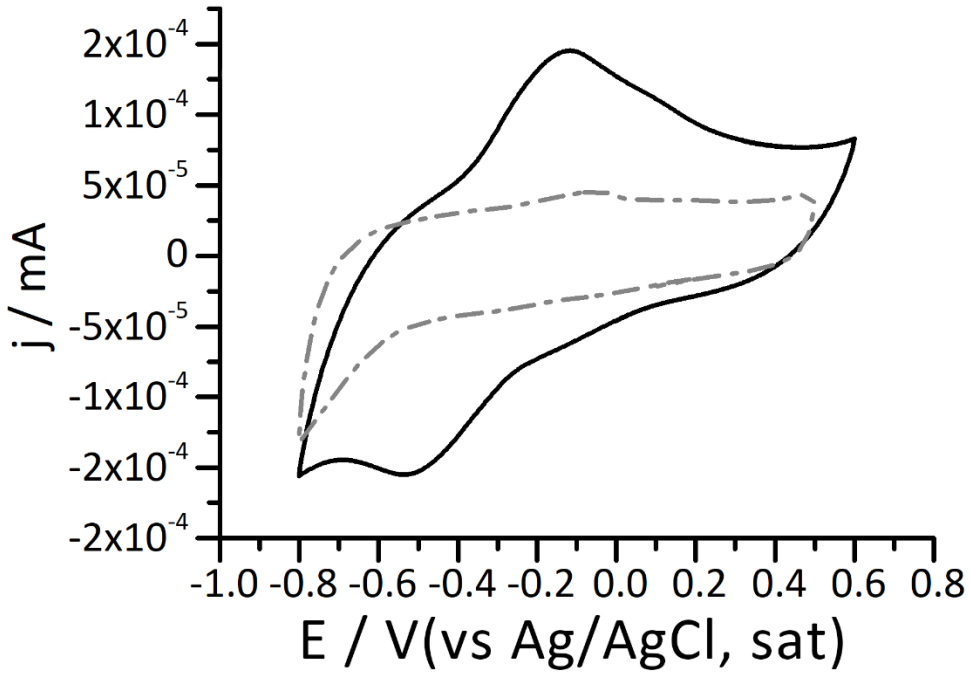

Figure S14. Voltammograms of bare graphite (gray trace) and graphite placed in direct contact with Fe_2O_3 particles (black curve).

Figure S14 shows voltammograms obtained on bare graphite and on a graphite electrode with Fe_2O_3 particles affixed at the electrode surface. In order to attach the particles a hole (1 cm depth x 0.05 cm width) was drilled at the electrode and loaded with ferric oxide powder. The resulting voltammogram is similar to that obtained in Figure S3 and shows broad oxidation and reduction peaks associated with Fe_2O_3 / Fe(II). These redox peaks with apparent midpoint potential close to -0.4 V vs Ag/AgCl (sat) are similar in form to that observed in Ferric Oxide MFC pilots.

Additional Polarisation Curves for Control and Ferric Oxide-enriched MFCs

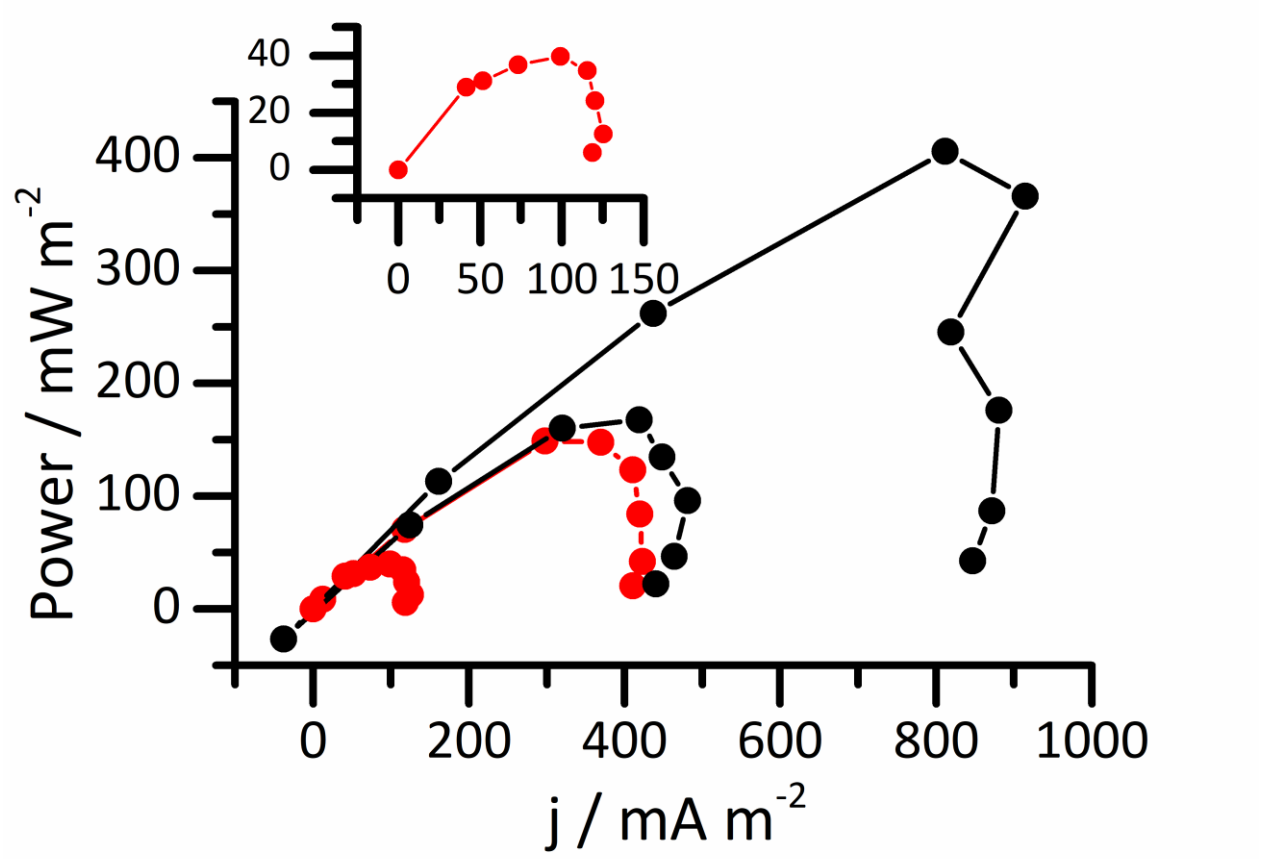

Figure S15. Additional MFC polarisation curves obtained after 30 days of bioanode incubation. Black: Control MFCs. Red: Ferric Oxide-enriched MFCs. The inset shows data in the range 0 – 150 mA m^{-2}

Voltammograms of Bioanodes After Biofilm Removal for DNA Extraction

Control and Ferric Oxide-enriched MFC bioanodes were analysed before (black traces in Figure S15) and 5 days after (red traces) biofilm removal for DNA extraction and 16S rRNA amplicon sequencing. Voltammograms prior to scraping off the biofilm show the expected catalytic acetate response for control pilots, while Ferric Oxide-enriched pilots show evidence of both the electroactive biofilm and of redox peaks attributed to the presence of adherent Fe_2O_3. After the biofilm is removed almost all catalytic acetate oxidation is absent from follow-up voltammograms, as is evidence of surface-attached Fe_2O_3. This suggests that the developing biofilm incorporates surrounding Fe_2O_3 as seen in SEM images of Ferric Oxide-enriched bioanodes above.

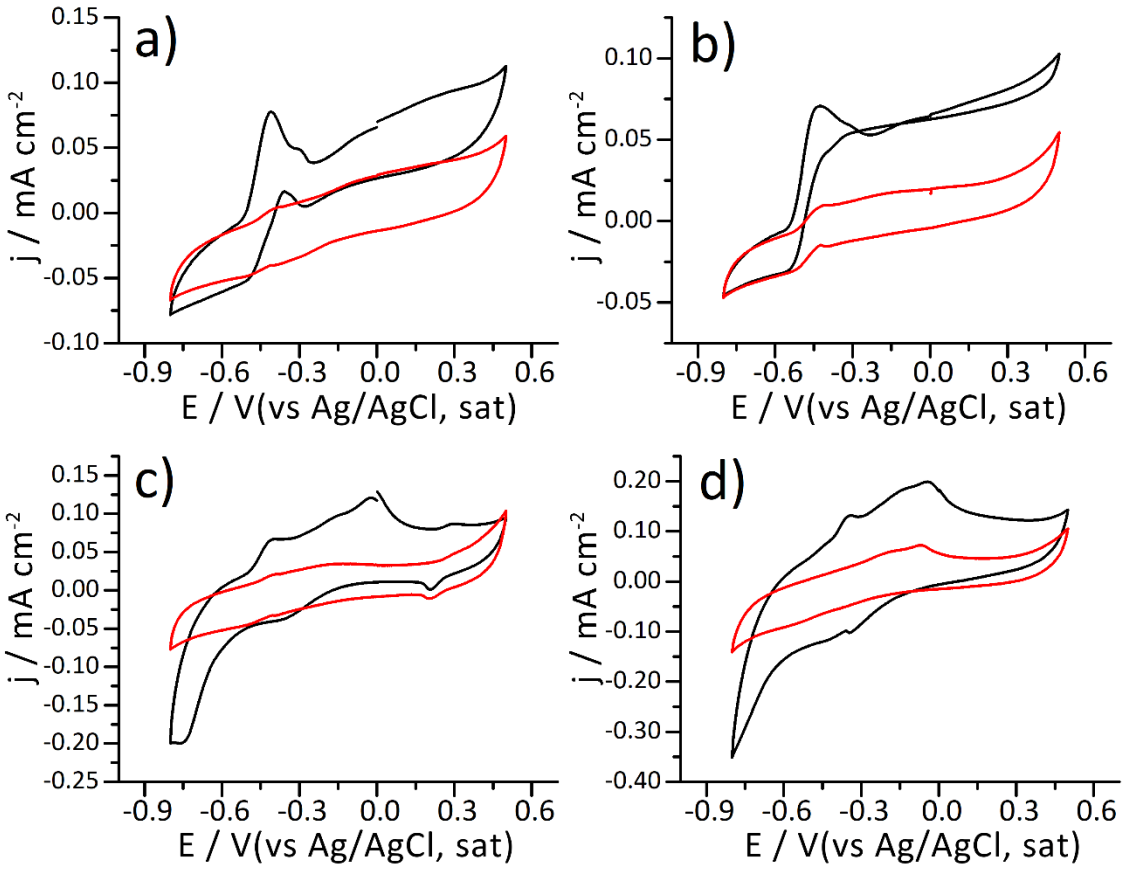

Figure S16. Voltammograms of a) b) Control MFC bioanodes and c) d) Ferric Oxide-enriched MFC bioanodes before (black trace) and after biofilm removal for DNA extraction experiments (red trace). Note that the voltammogram in b) is the same as that in Figure S5 a).

Community Analysis of Surrounding Inoculum

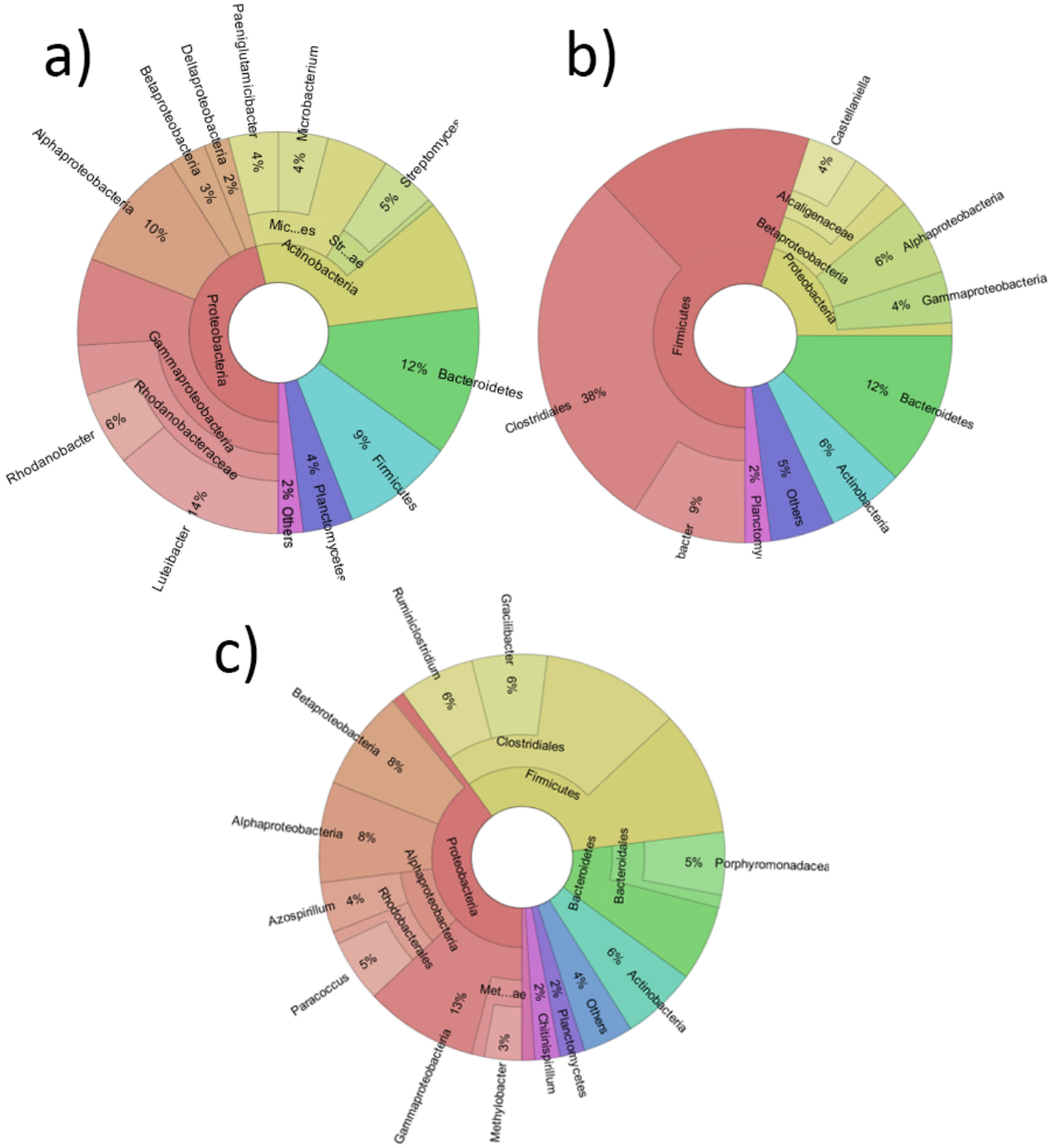

Figure S17. Community analysis of a) inoculum compost prior to incubation b) Control and c) Ferric Oxide MFC pilots after 54 days of continuous incubation in the presence of 10 mM acetate / 10 mM NaCl. Samples of anolyte and compost in close proximity to the bioanode surface were extracted and subjected to DNA extraction as described in the main text.